Building Technologies & Urban Systems Division
Energy Technologies Area
Lawrence Berkeley National Laboratory

Optimal design of microgrids to improve wildfire resilience for vulnerable communities at the wildland-urban interface

A.T.D. Perera[1,2], Bingyu Zhao[3], Zhe Wang [4,5], Kenichi Soga[6], Tianzhen Hong[2]

[1]Andlinger Center For Energy And Environment, Princeton University
[2]Building Technology and Urban Systems Division, Lawrence Berkeley National Laboratory
[3]Research Center for Transport Planning and Traffic Engineering, TU Wien
[4]HKUST Shenzhen-Hong Kong Collaborative Innovation Research Institute
[5]Department of Civil and Environmental Engineering, The Hong Kong University of Science and Technology
[6]Civil and Environmental Engineering, University of California Berkeley

Energy Technologies Area
February 2023

DOI: 10.1016/j.apenergy.2023.120744

This work was supported by the Assistant Secretary for Energy Efficiency and Renewable Energy, Building Technologies Office, of the US Department of Energy under Contract No. DE-AC02-05CH11231.

Optimal design of microgrids to improve wildfire resilience for vulnerable communities at the wildland-urban interface

A.T.D. Perera [a,b1], Bingyu Zhao[c], Zhe Wang [d,e], Kenichi Soga[f], Tianzhen Hong[b]

[a]Andlinger Center For Energy And Environment, Princeton University, NJ 08540, United States
[b]Building Technology and Urban Systems Division, Lawrence Berkeley National Laboratory, 1 Cyclotron Road, Berkeley, CA, 94720, United States
[c]Research Center for Transport Planning and Traffic Engineering, TU Wien, Vienna, Austria
[d]HKUST Shenzhen-Hong Kong Collaborative Innovation Research Institute, Futian, Shenzhen, China
[e]Department of Civil and Environmental Engineering, The Hong Kong University of Science and Technology, Hong Kong SAR, China
[f]Civil and Environmental Engineering, University of California Berkeley, Berkeley, CA, USA

Abstract

Climate change leads to extreme climate events that result in frequent wildfires that cause numerous adverse societal impacts. Public Safety Power Shutoffs, adopted by utilities to minimize the risk of wildfires, pose many challenges to electricity consumers. *Microgrids,* have been proposed to improve the resilience of energy infrastructure during wildfire events for vulnerable communities. However, a comprehensive techno-economic and environmental assessment of the potential of such energy systems have not been performed. To address this research gap, the present study introduces a modeling framework, consisting of (1) clustering algorithms that identify the communities based on building footprint data, fire hazard severity, and renewable energy potential; (2) a building simulation model to quantify the energy demand; and (3) an energy system optimization model to assist the *Microgrid* design. A novel optimization tool was introduced to model *Microgrid*s in wildland-urban interface, and subsequently, a comprehensive assessment was performed, focusing on seven localities from California, United States, with different climatic conditions. The study reveals that *Microgrid*s can keep the average levelized energy cost and annual Public Safety Power Shutoffs below $0.3/kilowatt-hour (kWh) and 2%–3% (of the annual energy demand), respectively. Furthermore, renewable energy penetration levels can be maintained above 60% of the annual energy demand. Therefore, *Microgrid* may become an attractive solution to reduce the adverse impacts of wildfires and enhance the resilience of energy infrastructure. However, the study reveals that *Microgrid* cannot completely eliminate the Public Safety Power Shutoffs. The levelized cost and renewable energy generation curtailments (waste of renewable energy) become notably high when attempting to eliminate Public Safety Power Shutoffs completely. A notable reduction in energy storage cost is essential to achieve zero Public Safety Power Shutoffs, and this is expected with the evolution of energy storage technologies. The present study recommends *Microgrids* for communities affected by wildfires to enhance the resilience of energy infrastructure and protect the health and safety of residents. The modeling framework and optimization tool developed in this study can be used by stakeholders and their consultants to inform design and optimization of *Microgrid*s for investment decision making.

Keywords

Wildfire, resilience; extreme climate events; microgrid; climate change, optimization

[1] Corresponding Author

Email:atdasun@gmail.com

Nomenclature

Sets

N decision spave variables
K objective functions
C constraints
O objects in the system such as wind turbines, PV panels etc
L the set of year considered for the lifetime
T the set of time steps in the time series

Parameters of the energy model

AM air mass value
A^{SPV} area of a single SPV panel
ELD_t electricity load demand
F_t^{ICG} fuel consumption of the ICG
G_t hourly solar irradiation
IG_{Lim} maximum power from the grid considering the grid curtailments
N^{SPV} number of SPV panels
P_t^a difference between energy demand and renewable energy generation
$P_t^{Bat-Max}$ maximum power flow from the battery
P^c critical Load
P^d dispatch load
$P_t^{ICG.Max}$ nominal power of the ICG
P_R rated power of the wind turbine
P_t^W net power generation from wind turbines
$\tilde{p}_t^W$ power generated by a single wind turbine
SOC state of charge
$SOC^{set\ point}$ state of charge set point
t time step $(t \in T)$
v_t wind speed at the hub level
v_R rated wind speed
v_{CI} cut-in wind speed
v_{CO} cut-off wind speed
W^G binary variable taking the value of 1 during the normal operation or 0 during the wildfire period.
x_t^1 normalized depth of discharge (DoD) of the battery bank
x_t^2 normalized load mismatch between demand and renewable energy generation
y_t part load of ICG
$\eta^{W\text{-losses}}$ losses that take place in the energy conversion of wind turbine
η_t^{SPV} efficiency of the solar panel
θ_t^{SPV} solar cell temperature

Parameters of the cost and CO2 model

CFG CO_2 intensity for the electricity unit taken from the grid
CICG CO_2 intensity of each unit generated by ICG
CRF capital recovery factor
GCT time-of-use tariff for power units selling
GCF time-of-use tariff for power units purchasing
l specific year of the lifetime ($l \in L$)
ICI initial capital investment
LOLP loss of load probability
$ICO2_o$ life cycle CO_2 emissions of a system component o ($o \in O$)
NPV Net present value
p real interest rate
o object in the system such as wind turbines, PV panels etc ($o \in O$).
OMF fixed operation and maintenance
p real interest rate
P_t^{SG} units sold to the grid
P_t^{IG} units purchased from the grid
OMV variable operation and maintenance cost

Other nomenclature

CHP combined heat and power
DOE Department of Energy, U.S.
HVAC heating, ventilation, and air conditioning
ICG Internal combustion generator
OPSP optimal power shutdown problem
PG&E Pacific Gas and Electricity Company
PV photovoltaic
PSPS Public Safety Power Shutoffs
TMY typical meteorological year
WUI Wildland-Urban Interfaces

1 Introduction

Climate change and anthropogenic alterations in forest lands have given rise to extreme wildfire incidents across the globe. According to a report by the United Nations [1], in the recent decade, record-breaking numbers of wildfires have occurred in regions not prone to extensive or prolonged fires in the past, such as eastern Australia, the Pacific Northwest, the Amazon, and the Arctic. The outcomes include significant disturbances to the local environment, safety, and economy, as well as contributions to the global warming cycle due to the release of carbon dioxide (CO_2) from burning.

Resilience and vulnerability of energy systems to future climate variations have been widely considered [2]. Ref. [3,4] discuss the climate resilience during heat waves. Sun et al. (2021) proposed using passive cooling designs to improve the heat resilience of residential buildings in disadvantaged communities [5]. Zeng et al. (2022) investigated the potential of using pre-cooling as a passive energy storage strategy to improve residential buildings' thermal resilience during heat waves [6]. In addition to heat waves, tornados and hurricanes might lead to severe consequences and need to be considered when designing the energy system of buildings. For instance, in 2017, the heating, ventilation, and air conditioning (HVAC) system of a nursing home lost power for three days due to Hurricane Irma, leading to 12 patients dying from excess indoor temperatures[7]. Sun et al. [8] examined the possibility of applying energy efficiency measures to enhance building thermal resilience under power outages due to tornadoes, hurricanes, and floods. Wildfire has also become increasingly frequent due to climate change, and severe outcomes may be expected when heat waves coincide with power outages such as the PSPS events in wildfire seasons, when the surging space cooling demand cannot be met by the power supply from the grid [9]. However, we did not find any studies focusing on energy system design considering wildfire risks.

Communities living at the border of urban and forest areas are known as Wildland-Urban Interfaces (WUI), and these are particularly susceptible to the negative impacts of wildfires. More than 46 million residents in 70,000 communities in the United States are at risk for WUI fires[10]. WUI neighborhoods are usually created by population growth that pushes property development to wildland areas. Building resilience against wildfire disasters in WUI areas depends on the cooperation of multiple infrastructure systems' functionalities, among which the energy system plays an important role. For example, a reliable electricity supply is needed to support residents' daily needs, telecommunications, traffic control and operations, and functioning of critical organizations such as hospitals in wildfire emergencies. However, the electricity system suffers from aging infrastructure and lack of resources in many WUI areas, so itself can pose a potential fire risk. At least 5 of the 20 most destructive California fires have been attributed to power line problems [11], including the 2018 Camp Fire, which claimed the lives of 85 people. Local utility companies are reacting to this by issuing Public Safety Power Shutoffs (PSPS), the emergency power cutoff on red flag warning days, as a means of preventing power lines from triggering a fire. This, however, inevitably impacts the functionality of other critical infrastructures in the WUI areas and causes disproportional difficulties to communities disadvantaged by limited access to the Internet, mobility, or existing health issues [12].

In search of a solution to improve the wildfire resilience in WUI areas, we evaluated the potential of using a microgrid in such areas by quantifying its reliability, cost, and environmental impacts. *Microgrid* is defined as a controllable and localized energy grid that can be disconnected from the regional grid and operate independently [13]. The aim of this research was to understand if microgrids can be economically feasible and reliable enough to provide electricity supply to WUI communities. A PSPS is a precautionary measure taken to reduce wildfire risks based on local weather forecasts (e.g., on "red flag days"). However, before fires break out, the PSPS may either directly impact the emergency power needs if a fire does occur, or the normal residential power needs without fire. Specifically, we chose to study the economic feasibility and reliability of microgrids in supplying the household energy needs in wildfire-prone communities, where the heating and cooling needs account for the majority of energy use. Loss of power for household cooling during heat waves can lead to severe consequences such as excess deaths [12], and heat waves are expected to be five- to ten-fold

more frequent by the end of this century [14]. Meanwhile, extreme heat is one of the leading causes of weather-related deaths in many places like California [15] and Europe[16]. A well-designed building energy system that can withstand these extreme events can play a major role in enhancing the climate resilience of buildings, limiting climate vulnerability, and mitigating the negative consequences of extreme weather conditions [17].

Wildfires driven by extreme climate conditions bring many challenges to the energy infrastructure [18,19]. Improving the resilience of energy infrastructure to such extreme events is a difficult task, requiring the assistance of integrated assessment models that combine climate and ecological models with the energy system and grid models [20]. Developing such a comprehensive, integrated model using bottom-up approaches (system models) has been difficult due to the complexities that arise when coupling these models. Therefore, most of the studies focused on arriving at localized solutions based on bottom-up approaches. The present state-of-the-art models on energy infrastructure resilience during wildfires have mainly focused on several aspects, including (1) quantifying the threat of triggering wildfire during extreme events, (2) deriving optimal power shutdown schedules during wildfire events, and (3) quantifying the impact of wildfires on building and transportation energy demand. Many studies have developed detailed thermal models to understand the threat of extreme climate events that cause wildfires [21–23]. Most of these methods are based on mathematical models. Meanwhile, Wischkaemper et al. [24] introduced an experimental approach to forecast the risks of wildfires caused by failing lines and apparatus. Based on such thermal models of wildfire risks, the optimal power shutdown problem (OPSP) [21,25–27] was formulated by combining the optimal power flow and the dispatch problems while taking into account power line shutdowns to reduce the threat of wildfires. Several formulations of OPSP are seen in the literature. For example, Trakas and Hatziargyriou [26] introduced a stochastic model to consider the uncertainties in the OPSP. Understanding the impact of wildfires on building and transportation energy demand plays a critical role when formulating the OPSP (third category). Hay & Mohit [28] discuss the impact of wildfires, taking into account the future scenarios for the building and transportation energy demand in the future. One of the main limitations of the current studies is that they have focused mainly on adapting existing energy infrastructure to improve resilience, specifically focusing on system operation. However, there are instances where adapting operation alone cannot guarantee a reliable electricity supply during extreme events. Design improvements that could help to withstand PSPS have not been taken into consideration.

Pacific Gas and Electricity Company (PG&E), a utility provider in California, USA, recently introduced microgrids to support the areas surrounded by wildfires [29,30]. These microgrids operate in the standalone mode during wildfire periods, which supplies the electricity demand for consumers without being dependent on the grid. In addition, these microgrids help to integrate renewable energy technologies, which will minimize the emission levels and support renewable energy integration with a minimal impact on the grid. In addition, a number of recent studies have demonstrated the potential of microgrids to improve energy resilience during wildfires [31–33]. For example, Yang et al. showed that power demand during the wildfire period could be reduced by up to 69.3% by using microgrids with diesel generators [32]. Hanna et al. also shows that diesel generators play a vital role in minimizing public safety power shutdowns using microgrids [34]. However, increasing the capacity of diesel generators can notably increase CO2 emissions [32]. On the other hand, replacing diesel generators with solar Photovoltiv (PV) and battery storage could notably increase the cost of the system according to Moreno et-al [33]. Therefore, an optimal balance between dispatchable generators, renewable energy generators and energy storage needs to be maintained within the microgrid, leading to a complex arrangement in the microgrid which needs to be designed considering its complex operation during grid-connected and standalone operation modes. Furthermore, none of these presents a comprehensive modeling framework to design such microgrids taking into account the energy demand, impact of wildfire and energy system optimization. Finally, most of the results obtained in these studies are highly specific to one location and it has been difficult to generalize these results. In order to address these bottlenecks, this study aims to achieve the following objectives:

- To introduce a modeling platform to optimize the design and operation of a microgrid that is resilient to wildfires
- To perform a techno-economic assessment to evaluate the economic burden of minimizing the PSPS-related power losses during wildfires by using microgrids for multiple communities in California
- To assess the environmental benefits of microgrids in minimizing carbon emissions
- To assess the role of renewable energy technologies (such as wind and solar energy), energy storage (battery banks), and dispatchable source (internal combustion generator [ICG]) in minimizing PSPS-related power losses, minimizing cost and reducing CO_2 emissions

Outcomes from the study can inform the planning and operation of utility resources to mitigate the impacts of wildfire events, especially for vulnerable communities. The modeling framework can be adopted by researchers and consultants to design and optimize GCEH.

The rest of the paper is organized as follows. Sections 2-4 present the methodology. Section 2 presents an overview of the methodology. It briefly presents the modeling theory and the computational methods used in the present study. Section 3 and 4 present an in-depth explanation of the elements of the computational platform. Section 3 presents a comprehensive building simulation model used to quantify the energy demand. Section 4 presents a detailed overview of the energy system optimization. Section 5 provides a comprehensive overview of the case studies where the methodology is applied. Section 6 presents a detailed techno-economic and environmental assessment of the energy systems. The limitations of the model and the conclusions are presented in Sections 7 and 8.

2 Methodology: Energy system optimization process

A microgrid operating in both standalone and grid-integrated modes was considered in the present study. The microgrid operates in the standalone mode during the period having a threat of wildfire, while it operates in the grid-integrated mode during the regular period. The microgrid consists of photovoltaic (PV) panels, wind turbines, an internal combustion generator, and a battery bank. The cooling and heating demand of buildings are supplied by air conditioners and heat pumps. Grid curtailments are considered for both selling and purchasing electricity to and from the grid during the grid operation. The time-of-use tariff system was used when computing the cost of grid interactions. The configuration used in the present study matches with the configuration suggested in the present state-of-the-art microgrids that are used to enhance the resilience for wildfire [33]. In addition to the renewable energy technologies, an internal combustion generator is used to minimize cost while enhancing renewable energy utilization and reliability. The role of internal combustion generators has been widely discussed in the previous publications of the authors [35,36].

Fig. 1 shows the workflow of this study, which includes three major steps: (1) selecting communities to be studied through clustering and wildfire risk evaluation, (2) building energy demand simulation, and (3) microgrid optimization. Specifically, the building energy demand was profiled for the selected communities based on the unique building and weather conditions of each, and the calculated building energy demand was the input of the subsequent energy system design calculation. The rest of this section introduces the theories behind each modeling step, and other details are given, along with the case study in Section 4.

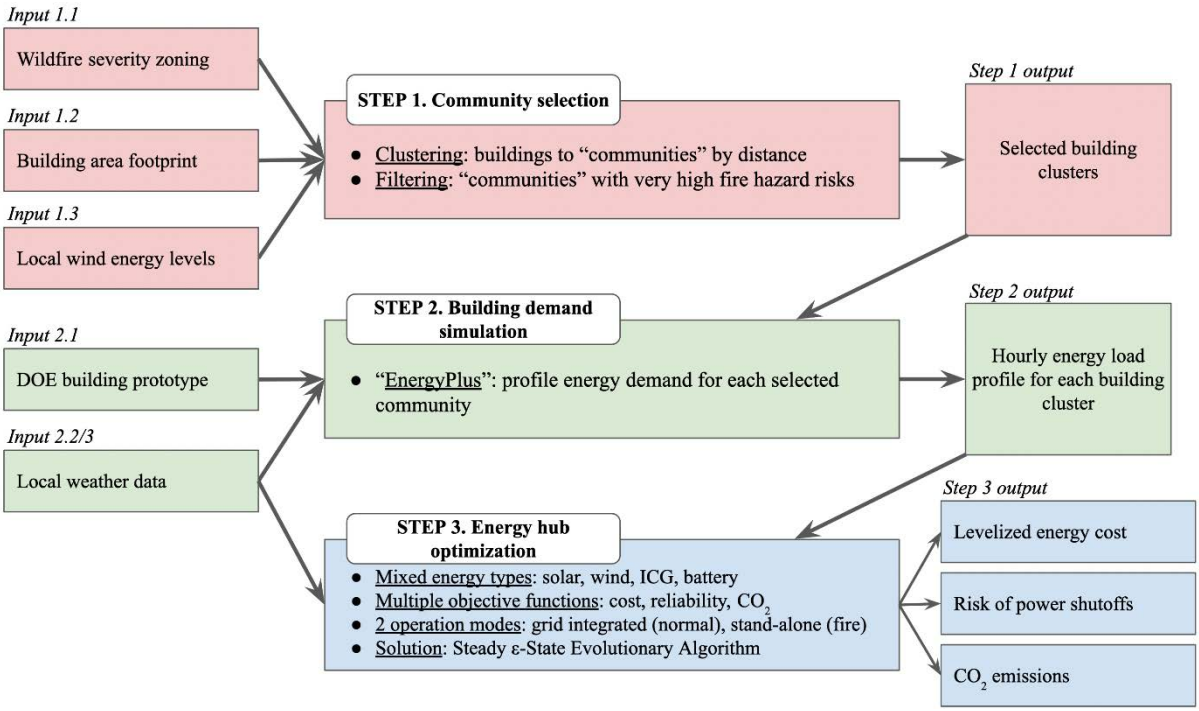

Fig. 1: Platform used to design microgrids to improve the resilience of communities at the Wildland-Urban Interface

3 Building energy demand simulation

We used EnergyPlus to generate the building electricity load profiles. The workflow is shown in Fig. 2. We used the U.S. Department of Energy (DOE) prototype model for single family houses [37] to represent the typical residential building in California. The thermal parameters of the building envelope (e.g., the U-value of the exterior walls, U-value and solar heat gain coefficient [SHGC] of windows) were selected based on the climate zone where the community is located. We used typical meteorological year (TMY) weather files downloaded from https://energyplus.net/ in the EnergyPlus simulations. There are 59 weather files recorded from 59 weather stations in California in total. We used the haversine function to find the closest weather station for each community. The building's electricity load highly depends on the heating system type. In this study, we simulated the three heating system types most widely used in California. The building model, weather file, and building energy system were inputted to EnergyPlus to generate the hourly building load of the six communities selected in this study (described in Section 5).

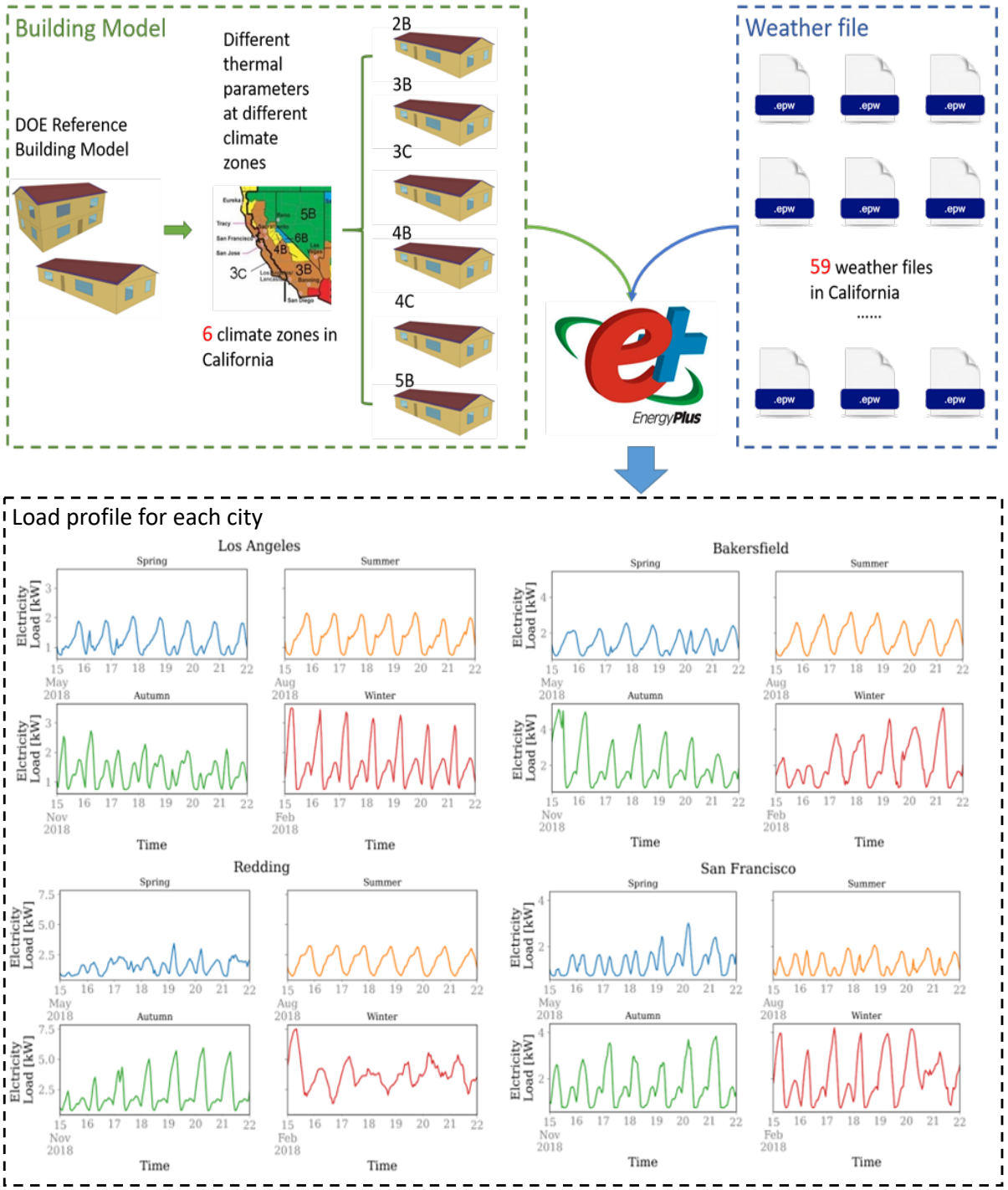

Fig. 2: Workflow used for the building simulation: we modeled the 6 climate zones in California, i.e.: 2B, 3B, 3C, 4B, 4C, 5B

4 Formulating energy generation/conversion within the microgrid

4.1 Solar energy component

Hourly time series potentials for solar energy and wind energy are taken as the inputs for the energy system model. Both solar irradiation and wind speed data are taken from the closest meteorological station. Based on the hourly solar irradiation G, air mass value (AM) [27] and solar cell temperature

(θ_t^{SPV}), the efficiency (η_t^{SPV}) of the solar panel is computed for the time step $t(t \in T : set\ of\ all\ hours\ in\ the\ year)$ by the model proposed by Durisch et al. [26] (Eq. 1).

$$\eta_t^{SPV} = p^{SPV}\left[\mathrm{q}^{\mathrm{SPV}}\left(\frac{G_t}{G_0}\right)+\left(\frac{G_t}{G_0}\right)^{m^{SPV}}\right]\left[1+r^{SPV}\left(\frac{\theta_t^{SPV}}{\theta_0^{SPV}}\right)+s^{SPV}\left(\frac{AM}{AM_0}\right)+\left(\frac{AM}{AM_0}\right)^{u^{SPV}}\right],\ \forall t \in T \quad (1)$$

In this equation, values for G_0, θ_0^{SPV}, and AM_0 are taken respectively as G_0 = 1,000 Wm-2, θ_0^{SPV} = 25°C and AM_0 = 1.5. Parameter values of p^{SPV}, $\mathrm{q}^{\mathrm{SPV}}$, r^{SPV}, s^{SPV}, m^{SPV}, u^{SPV} for different solar photovoltaic (SPV) technologies, such as mono-crystalline, polycrystalline, and amorphous silicon cells, are taken from Ref. [38]. Subsequently, power generation using PV panels is calculated using Eq. 2.

$$P_t^{SPV} = G_t\ \eta_t^{SPV}\ A^{SPV} N^{SPV},\ \ \forall t \in T \quad (2)$$

In this equation, A^{SPV} and $N^{SPV}\ (N^{SPV} \in \mathrm{N})$ present the area of a single SPV panel and the number of SPV panels.

4.2 Wind energy component

Wind power generation is computed in a similar way as SPV generation. We have considered horizontal axis wind turbines in the present study. Time series of hourly wind speed at 10 meters (m) anemometer height is taken as the input to compute the wind speed at the hub level (v_t) and to calculate the wind energy generated from wind turbines using a power law approximation. n_s represents the number of cubic spline interpolation functions [39,40], and (n_s+1) points are used to approximate the power curve of the wind turbine (taken from the manufacturer), which leads to Eq. 3.

$$\tilde{P}_t^{w} = \begin{cases} \tilde{P}_t^{w} = 0, & v_{CI} > v_t \\ \tilde{P}_t^{w} = a_1^{w} v_t^3 + b_1^{w} v_t^2 + c_1^{w} v_t + d_1^{w}, & v_{CI} < v_t < v_1 \\ \tilde{P}_t^{w} = a_2^{w} v_t^3 + b_2^{w} v_t^2 + c_2^{w} v_t + d_2^{w}, & v_1 < v_t < v_2 \\ \quad\cdots\cdots\cdots & \\ \quad\cdots\cdots\cdots & \\ \tilde{P}_t^{w} = a_{n_s}^{w} v_t^3 + b_{n_s}^{w} v_t^2 + c_{n_s}^{w} v_t + d_{n_s}^{w}, & v_{n_s-1} < v_t < v_{n_s}(v_R) \\ \tilde{P}_t^{w} = P_R, & v_R < v_t < v_{CO} \\ \tilde{P}_t^{w} = 0, & v_t > v_{CO} \end{cases}, \forall t \in T \quad (3)$$

In Eq. 3, a_i^{w}, b_i^{w}, c_i^{w}, and d_i^{w} are coefficients of the polynomial function, which vary depending on the "power curve." v_R, v_{CI}, v_{CO}, and P_R denote rated wind speed, cut-in wind speed, cut-off wind speed, and rated power of the wind turbine. Finally, net power generation (P_t^{W}) is calculated using Eq. 4.

$$P_t^{W} = \tilde{P}_t^{W}(\mathrm{v_t})\ \mathrm{N^w}\ \eta^{\mathrm{W\text{-}losses}}, \forall t \in T \quad (4)$$

In Eq. 4, $N^{W}\ (N^{W} \in \mathrm{N})$ denotes the number of wind turbines, which is optimized using the optimization algorithm. $\tilde{p}_t^{W}$ denotes power generated by one wind turbine calculated using the power curve and $\eta^{\mathrm{W\text{-}losses}}$ accounts for other losses that take place in the energy conversion.

4.3 Internal combustion generator (ICG) component

The ICG operates as the dispatchable energy source. The operation of the ICG is determined by the dispatch strategy described comprehensively later in this section. The fuel consumption of the ICG (F_t^{ICG}) is formulated as a polynomial function of the part load (y_t), as presented in Eq. 5 [41].

$$F_t^{ICG} = \sum_{\forall t \in T} a_k^{ICG} + b_k^{ICG}\, y_t + c_k^{ICG}\, y_t^2 + d_k^{ICG}\, y_t^3 + e_k^{ICG}\, y_t^4, \forall t \in T \quad (5)$$

In this equation, a_k^{ICG}, b_k^{ICG}, c_k^{ICG}, d_k^{ICG}, and e_k^{ICG} are taken from the performance curve of the kth ICG, $k(k \in \mathrm{N})$, obtained from the optimization algorithm. In this equation, y_t denotes the operating load factor of ICG. Fuel consumption is used when computing the operational cost of the system.

4.4 Battery bank component

The battery bank is used for energy storage. The operating conditions of the battery bank (the decisions for charging and discharging) are taken from the dispatch strategy. The state of charge (SOC) is determined depending on the charging and discharging process according to Eq. 6 [42].

$$\mathrm{SOC_{t+1}} = \mathrm{SOC_t(t).}\left(1 - \sigma^{\mathrm{bat}}{}_{\mathrm{t}}\right) + V_{\mathrm{bat}}\mathrm{I_{bat_t}}\Delta\mathrm{t.}\,\eta_{\mathrm{ch_t}}/\mathrm{C_{bat}} \quad (6)$$

In Eq. 6, σ^{bat} denotes the self-discharge coefficient, which was taken as 0.02%, η_{chg} and C_{bat} denote the round cycle efficiency of the battery bank and its capacity (which depends on the number of battery banks N^{Bat} ($N^{Bat} \epsilon \mathbb{N}$) optimized using the optimization algorithm). V_{bat} and $\mathrm{I_{bat_t}}$ denote voltage across the battery bank and current flow during the Δt time step (taken as one hour). The Rain-Flow algorithm is used to derive the battery life cycle based on charging and discharging cycles [43]. Based on the number of batteries in the battery bank and the replacements, the life cycle cost of the battery storage is computed.

4.5 Dispatch strategy and simulation

Hourly (short-term) and seasonal (long-term) variations in the energy demand, renewable energy potential, and grid prices have a notable impact on the operations of the energy system and thus influence its configuration [36]. Dispatchable energy technologies such as combined heat and power (CHP) and ICG, and energy storage technologies such as battery banks, are important system components, and decisions regarding their operational strategies need to be designed carefully. The choice of management strategy adapted for a particular time step affects the temporal operational cost and subsequent operational decisions. Therefore, life cycle simulation is required at the design stage. The impact of the dispatch strategy on the system sizing problem makes it challenging to design distributed energy systems. Furthermore, designing wildfire-resilient energy systems adds to the challenges, since the system needs to operate in two distinctly different modes: during wildfire PSPS incidents and during normal conditions. During the PSPS events, the microgrid needs to operate as a standalone energy system, as the main grid will be cut off. In normal operating conditions, however, the system operates in the grid-integrated mode. Although a more comprehensive assessment of the dispatch strategy can be assessed using machine learning techniques such as reinforcement learning [44,45], it increases the computational burdens exponentially in the design process. Therefore, a simplified dispatch strategy that can easily couple with optimization techniques is deemed more appropriate. A plethora of methods used in this context are reported in Ref. [46]

A two-stage dispatch strategy was used in the present study to consider the operation of the system in its grid integrated and standalone modes. Specifically, a bi-level dispatch strategy introduced by

Perera et al. [47] was used for the grid integrated mode. During the standalone mode, the dispatch strategy adopted was adapted from Lopez et al. [48] and Perera et al. [42,49]. A comprehensive description of these two dispatch strategies is presented in Section 5.3.1 and 5.3.2, respectively.

4.5.1 Stage 1: Grid integrated operational mode (Normal operation)

The dispatch strategy contains two levels. The primary level determines the operating load factor of the ICG, while the secondary level determines the charge/discharge levels of energy storage and grid interactions.

Two input variables, x_t^1 and x_t^2, are used, which denote the normalized depth of discharge (DoD) of the battery bank and the normalized load mismatch between demand and renewable energy generation. The operating load factor of the ICG (y_t) is determined according to Eq. 7 [47].

$$y_t = \frac{P_t^{ELD} - P_t^{RE}}{\max_{\forall t \in T}(P_t^{ELD} - P_t^{RE})} \tag{7}$$

In Eq. 7, P_t^{ELD} and P_t^{RE} denote the electricity demand and renewable energy generation, respectively. A similar approach is used to compute the normalized DoD. Finally, the load factor of the ICG is determined using the Takagi-Sugino method [50–52], based on x_t^1 and x_t^2.

The secondary level focuses on the operating conditions of the energy storage and grid interactions. It is based on finite state automata, where the system is expected to operate in eight main operating states. The critical parameters that define the states are optimized along with the system design. Combined Dispatch Strategy, which is a combination of Battery Charging Strategy, Frugal Discharge Strategy, SOC Set Point Strategy, Load Following Strategy, and Peak Shaving Strategy is used in this work [10,35,36]. A detailed description of the Dispatch Strategy is illustrated in this section. A comprehensive overview of Stage 1 can be found in Ref. [47,53].

4.5.2 Stage 2: Standalone operational mode (Wildfire operation)

Stage 2 of the dispatch is based on the combined dispatch strategy proposed by Lopez et al. [48] and Perera et al. [42,49]. It uses a combination of basic operational strategies for standalone hybrid energy systems proposed by Barley and Winn [54]. During Stage 2, the system does not have any interactions with the grid. Therefore, it depends on ICG, energy storage, and renewable energy technologies when supplying the energy demand. Stage 2 is based on finite automata theory, and five main operating states (based on main dispatch strategies introduced by Barley and Winn [54]) are used.

State 1: Battery Charging Strategy

When renewable energy generation is higher than the demand, the battery charging strategy is adapted where excess generation is charged into the battery bank. Any excess generation that exceeds the capacity of the battery bank is dumped as wasted energy.

State 2: Frugal Discharge Strategy

The frugal discharge strategy is used when the energy demand is higher than the renewable energy generation, but the difference between energy demand and renewable energy generation (P_t^a) is small. When the dispatchable energy sources such as ICG or gas turbine operates at very low load factors, the operating lifetime can be reduced notably. At the same time, their fuel efficiency also deteriorates significantly. Therefore, a battery bank is used to cater to such demands. However, discharging the battery bank to a very low state of change will lead to a reduction in battery lifetime. Therefore, the frugal discharge strategy is only adopted when P_t^a is less than a critical maximum

amount known as the dispatch load (P^d). The optimal value for the dispatch load is obtained from the optimization.

State 3: SOC Set Point Strategy

When the demand exceeds the renewable power generation by P^d or higher, the system moves into State 3. In the Set Point Strategy, the ICG is driven at the maximum power, which helps to improve its lifetime and fuel efficiency. The additional power generated by the ICG is used to charge the battery bank. However, charging the battery bank using the ICG has an opportunity cost (since it can be charged freely using the renewables). Therefore, a maximum value is set for the battery energy level to be charged through ICG, known as a state of charge set point ($SOC^{set\ point}$). The $SOC^{set\ point}$ is obtained through the optimization process introduced in Section 5.4.

State 4: Load Following Strategy

Charging the battery bank using the ICG has several disadvantages, mentioned previously. Therefore, the system will shift to the load-following strategy, where the ICG provides the mismatch between the demand and generation and is not used to charge the battery bank, when P_t^a is greater than a certain threshold, known as the Critical Load (P^c).

Sate 5: Peak Shaving Strategy

Finally, when P_t^a is greater than the nominal power of the ICG, a battery bank is also used, along with the ICG. There will be a loss of power supply whenever both the ICG and the battery bank cannot cater to the mismatch P_t^a .

4.6 Formulation of objective functions and constraints

A Pareto optimization was performed in the present study by taking a set of objective functions. This section presents the formulation of the objective functions.

4.6.1 Power supply reliability

A drop in the power supply could take place mainly during the wildfire season, when the operation of the grid is terminated to minimize wildfire risk in PSPS events. Microgrids can assist in such scenarios. However, a portion of the energy demand needs to be curtailed in instances when the energy demand is higher than the energy from renewable energy generation, ICG, and battery combined. Based on that, loss of power supply is formulated according to Eq. 8.

$$LPS_t = P_t^{ELD} - P_t^{RE} - P_t^{ICG.Max} - P_t^{Bat-Max} - W^G\, IG_{Lim}, \forall t \in T \tag{8}$$

In this equation, ELD_t, $P_t^{ICG.Max}$, $P_t^{Bat-Max}$, denote electricity load demand, nominal power of the ICG, and maximum power flow from the battery depending upon the state of charge, respectively. W^G is a binary variable taking the value of 1 during the normal operation or 0 during the wildfire period. Finally, IG_{Lim} represents the maximum power from the grid considering the grid curtailments.

Power supply reliability is calculated in this study using the loss of load probability (LOLP) model, as in Ref. [55–58]. Loss of load occurs whenever power generation within the system is less than the demand (according to Eq. 10) and the mismatch cannot be supplied by both the battery bank (due to the limitations in energy storage) and the grid (due to the grid curtailments).

The LOLP is calculated using LPS according to Eq. 9. It is a performance indicator to evaluate the power supply reliability.

$$LOLP = \frac{\sum_{\forall t \in T} LPS_t}{\sum_{\forall t \in T} P_t^{ELD}}, \forall t \in T \quad (9)$$

4.6.2 Grid integration level

Strong interactions with the main utility grid will make the microgrid vulnerable during the wildfire period. Therefore, the autonomy of the microgrid is an essential performance indicator that can be defined in a number of different ways. In the present study, we used the formulation presented in Eq. 10 based on Ref. [47].

$$GI = \sum_{\forall t \in T} P_t^{IG} / \sum_{\forall t \in T} P_t^{ELD}, \forall t \in T \quad (10)$$

In this equation, P_t^{IG} denotes the energy units purchased from the grid. In addition, grid curtailments for both injection and purchase are considered in this study as a practice to maintain the stability of the grid.

4.6.3 Net present value of the system

Net present value (NPV) of the system is considered to be a performance indicator in the assessment. NPV consists of initial capital investment (ICI) and operation and maintenance costs. The ICI consists of both the acquisition and installation costs of wind turbines, SPV panels, the battery bank, the ICG, power electronic devices, and other equipment) for system components. The operation and maintenance cost consists of two components: (1) the fixed operation and maintenance (OMF) cost and (2) the variable operation and maintenance cost (OMV). OMF accounts for costs of the maintenance of wind turbines, SPV panels, fuel and operational costs for ICG, etc., while OMV accounts for replacement costs for the ICG and battery bank (which were determined based on their operation). NPV is formulated as Eq. 11 [53].

$$NPV = ICI + \sum_{\forall o \in O} (OMF_o\, CRF_o) + \sum_{l=1}^{L} \sum_{\forall o \in O} p^l OMV_{o,l} + CRF_G \sum_{\forall t \in T} (P_t^{IG} GCF_t - P_t^{SG} GCT_t), o \in O, \forall t \in T, l \in L \quad (11)$$

In this equation, *CRF, p, GCT ,* and *GCF* denote the capital recovery factor, real inflation, time-of-use tariff for power units selling back to the grid, and price of grid electricity when purchasing electricity and selling it back, respectively. In the equation, o($o \in O$) presents an object in the system such as wind turbines, PV panels etc. P_t^{SG} presents the units sold to the grid and l($l \in L$) indicates the year.

4.6.4 Levelized CO_2 emissions

The solution incorporates sustainability considerations in its design. Levelized CO_2 emissions are taken as a system sustainability performance indicator. The total CO_2 emissions are computed by taking into account embedded CO_2 emissions for system components, CO_2 emissions during ICG operation, and the CO_2 emissions for grid electricity (Eq. 12) [53].

$$CO_2 = \sum_{\forall o \in O} ICO2_o + L \sum_{\forall t \in T} (P_t^{IG}\, CGF_t + CICG_{t,y_t} P_t^{ICG}), o \in O, \forall t \in T \quad (12)$$

In this equation, *ICO2$_o$* (kilograms, kg) denote the life cycle CO_2 emissions of a system component o ($o \in O$), including a replacement for the ICG and battery bank. *CFG* [kg/kWh] denotes the CO_2 intensity for the electricity unit taken from the grid, and *CICG* [kg/kWh] denotes the CO_2 intensity of each unit generated by ICG depending upon the load factor of the ICG.

4.7 Optimization algorithm

A number of methods based on different approaches have been proposed to optimize distributed energy systems. Some of these methods are well suited for standalone applications, while others are more often used for grid integrated operational mode. The uniqueness of the present case is that the system needs to operate in both grid-connected and standalone mode. Based on the previous work of the authors on both grid-connected and standalone applications, a heuristic algorithm is used to optimize the configuration of the energy system, along with the dispatch strategy. Both system configuration and operational strategy are the decision space variables. The decision space variables related to the dispatch strategy cover both the grid integrated mode and the standalone operational mode. NPV, CO_2 emissions, loss of load probability, and grid integration level are considered as objective functions. The decision space variables are mapped into the objective space through a simulation-based model (a simulation-based optimization). Hourly renewable energy potential, energy demand, and grid prices are taken as the input. The dispatch strategy determines the operating conditions of the ICG depending on whether the system is operating in grid-connected or standalone mode. Based on the energy demand, renewable and dispatchable energy generation, the interactions between the grid (only in the grid-connected mode) and the battery bank are determined. In a similar manner, the system is simulated for the entire 8760 time-steps, which enables to match the decision space variables into the objective space in a similar manner presented in Ref. [47].

A Steady ε-State Evolutionary Algorithm [59] is used in this study for updating the archive and reproduction of the population, which is proven as a method to maintain diversity while reaching the final set of Pareto solutions within a short period of time. A polynomial mutation operator [60] and simulated binary crossover operator [61] are used along with differential evolutionary operators [77]–[79] in the reproduction of the population. The constraint tournament method [60] is used to handle the constraints in the optimization algorithm. The optimization code is implemented in the C++ Visual Studio platform. The paper presents an extension to the model used in Ref. [65] and [66]. Therefore, the application of the optimization model is quite straightforward. A detailed discussion about the use of heuristic algorithms for complex optimization processes with microgirds (based on the present optimization algorithm) is presented for scenarios including the game theory [67,68], stochastic optimization [41], robust optimization[69], and a large pool of decision space [44].

5 Case study

5.1 Screening of eligible communities in wildfire-prone areas in California

The case study was situated in fire-prone areas of California. In choosing a suitable location that satisfied the microgrid system requirements, we developed an automatic community clustering and filtering algorithm that takes in inputs of multiple map layers (building footprints, wildfire risks, wind resources) and generates locations/communities suitable for microgrid systems to be adopted. The process (corresponding to Step 1 in Fig. 1) is shown in Fig. 3 below.

A suitable community (group of energy-consumption buildings) for microgrid implementation meets the following criteria:

1. The size of the community does not exceed 1 kilometer square, given the equipment restrictions for microgrid.
2. The number of buildings in the community is preferably less than 100, given the installation difficulty of the microgrid.
3. The community should be in fire-prone areas that may suffer from PSPS or similar power cutoff events from the utility providers.
4. The community should have a sufficient supply of alternative energy to support the microgrid power generation.

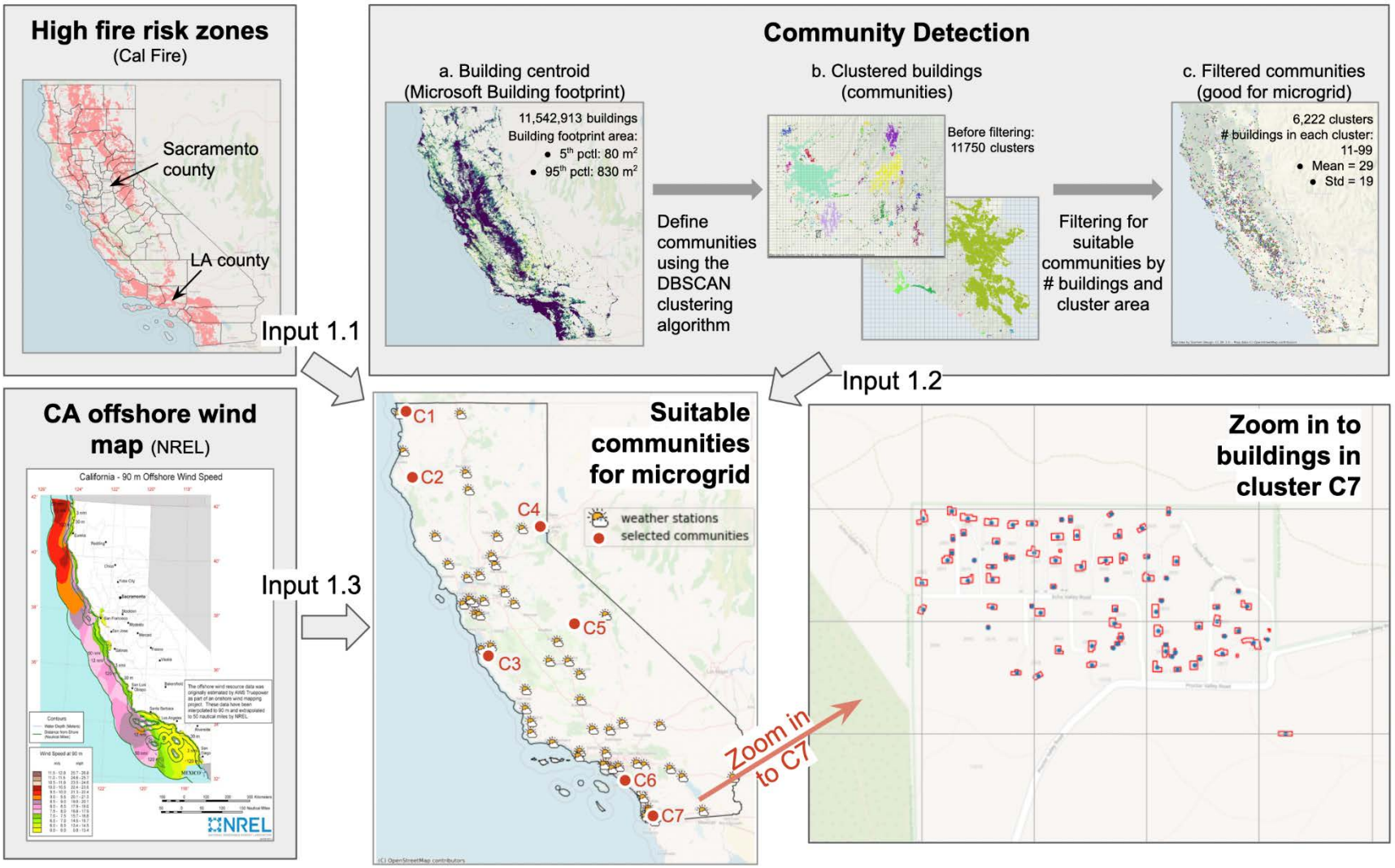

Fig. 3: The process of selecting suitable communities for installing microgrid.

Based on such criteria, three types of inputs were collected for the case study area of California. These included: (1) the building footprint map from Microsoft [70]; (2) the Very High Fire Hazard Severity Zone (VHFHSZ) classification from CAL FIRE [71]; and (3) the National Renewable Energy Laboratory (NREL) offshore wind energy map [72]. Several clustering algorithms and parameters have been tested on the building footprint data, and the Density-Based Spatial Clustering of Applications with Noise (DBSCAN) algorithm with a threshold parameter of 500 leads to the best outcome in terms of community detection (Fig. 3(b)). The clustered buildings were then filtered only to keep those that satisfied criteria 1 and 2 above. Altogether, there are 6,222 such clusters (relatively detached and compact communities with <100 buildings) in California, and these are mainly remote villages or farms. Next, the filtered communities were clipped by the VHFHSZ map to find those with at least 80% of the buildings in the VHFHSZ, indicating high risks of fire and power loss under extreme weather conditions. This led to 1,424 communities. The framework here provides an automated process to find suitable communities for microgrid implementation across large geographical areas, but only seven communities were chosen to demonstrate the methodology of the benefit quantification using the energy system optimization model, labeled C1–C7 in Section 4.3. The chosen communities are also close to weather stations, guaranteeing the accuracy of the energy demand modeling in the next section.

The socioeconomic status of the communities, compared against the cost of installing the microgrid system, was not considered in this research. Foreseeably, only affluent communities (e.g., large resorts or businesses) may afford such a system. Nevertheless, we aim to provide an estimation of the benefits of adopting the microgrid under repeated wildfires and unreliable energy supplies in the WUI area, which may lead to policy discussions by stakeholders.

5.2 Wildfire period and energy demand

In this study, the building loads for four representative clusters (C3, C4, C5, and C7) were analyzed for a 12-month cycle, to account for a year-round fire season case in California. In the analysis below (Fig. 4), *Spring* is defined as March to May; *Summer* is June to August; *Autumn* is September to November; and *Winter* is from December to February. The major contributor to the load profile difference is the local climate of the communities. For example, Cluster C4 is close to Lake Tahoe, which has a cool summer, therefore has a relatively small cooling load in summer and autumn. On the contrary, Cluster C5 is close to Fresno, which has a hot summer and cold winter, and the energy demand throughout the year is the highest among the four selected clusters.

Next, we selected Cluster C7 to analyze the temporal load variability within a day in each season, assuming an air source heat pump is used for heating. Heating and cooling electricity consumption is high for Cluster C7. The peak load happens at about 6 pm in summer and autumn as people return home from work and turn on electrical devices for air conditioning, cooking, and entertainment. Meanwhile, the cooling demand in the late afternoon and early evening is high because of the relatively high ambient temperature and the heat stored in the thermal mass during the daytime. In winter, for residential buildings in the selected community, electricity usage is the highest in the early mornings, primarily because people wake up and turn on electrical devices for preparing breakfast, using lighting and other energy-consuming devices. In spring, there is a dual peak in the early morning and at sunset, however the peak is not as high as that in Winter and Summer.

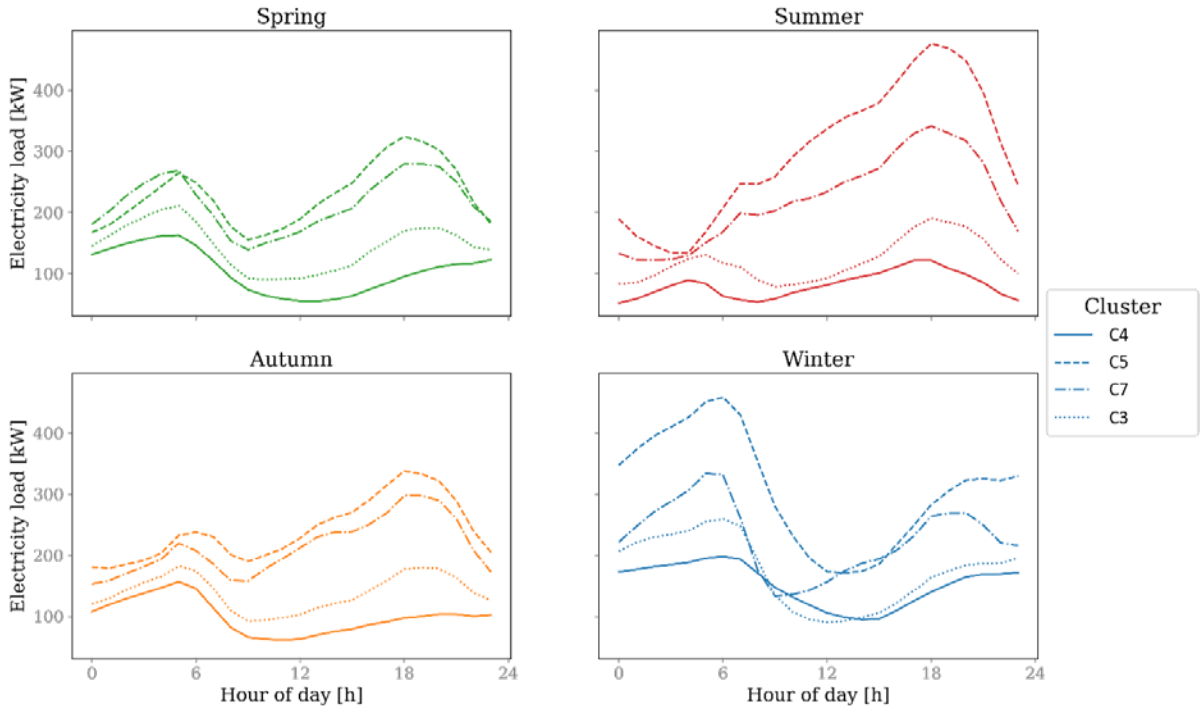

(a)

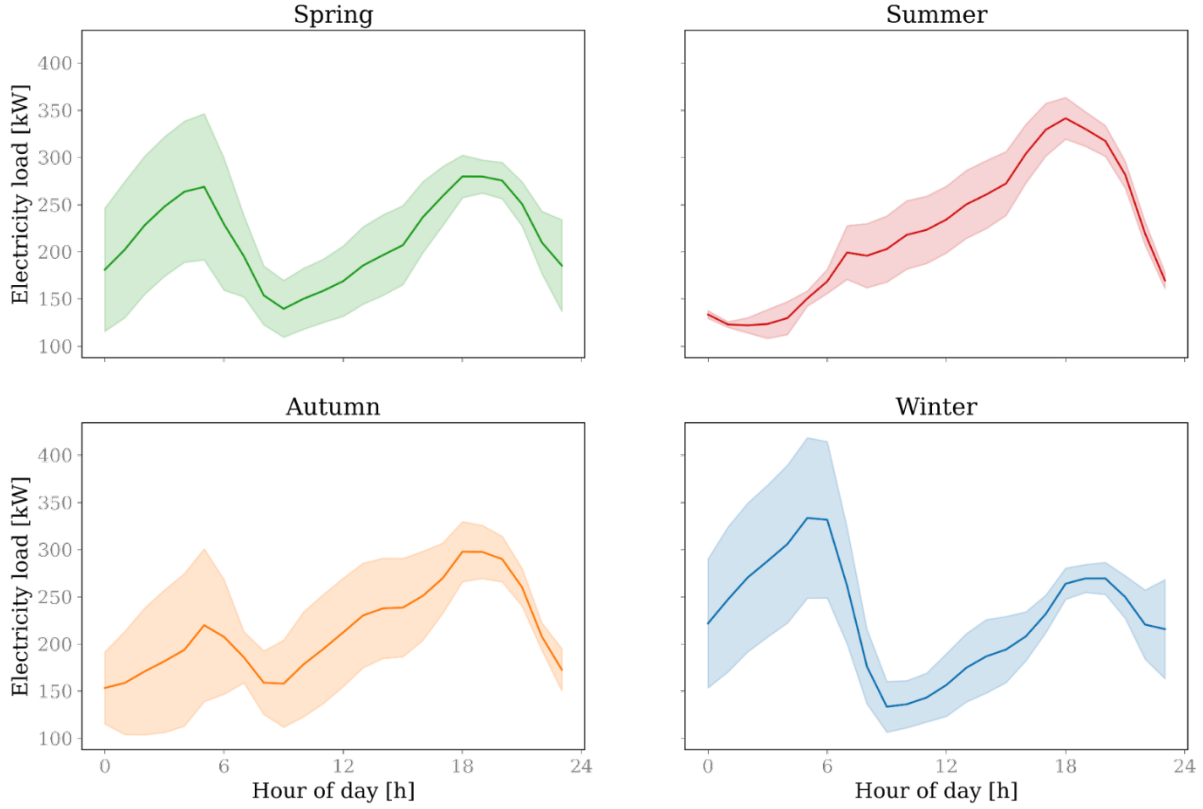

(b)

Fig. 4: The variation of the energy demand, depending on (a) location and (b) season

It is worth mentioning that the load profile greatly depends on the household heating method. In this study, we considered three major heating options: (1) gas boiler, (2) electrical heating that directly converts electrical energy to heat, and (3) air source heat pump, which uses heat pump technologies to improve heating efficiency. Gas boiler is the most widely used solution for heating in California now, which can be referred to as Business As Usual (BAU) scenario. As shown in Fig. 5, the gas boiler leads to the least electricity consumption, as heating is provided by natural gas. In this case, the electricity consumption peak happens at about sunset in all four seasons. The electrification campaign in California requires that the new constructions, including the residential houses, can only use electricity rather than any other fossil fuels in buildings, leaving two options for heating – electrical heating and air source heat pump. Using electrical heating significantly improves the daily electricity consumption, especially in spring and winter. Electrical heating is a cheaper and mature technology, however its energy efficiency is low. Using an air source heat pump can significantly reduce the electricity consumption due to its high energy efficiency. As there is no heating demand in summer, the load curves of the three heating options are close to each other in summer.

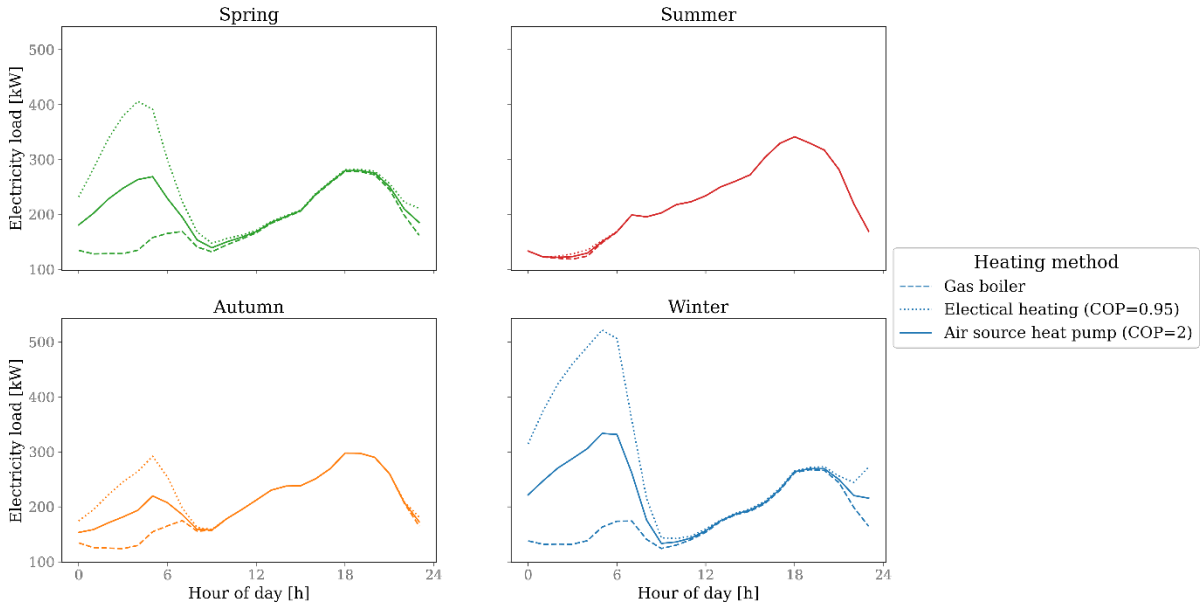

Fig. 5: Typical load pattern with different heating options

We selected the air source heat pump case for the subsequent optimization analysis for two reasons. First, to address the climate change crisis, the California government is promoting the electrification of residential buildings, requiring that new residential buildings only use electricity as the energy source, thus excluding gas boilers from being installed in the future. Second, air source heat pumps are becoming increasingly popular for space heating due to their high energy efficiency. Therefore, the air source heat pump case will be the dominating heating method in California. Because of these two reasons, we decided to narrow down to the specific scenario where heat pumps are used to generate heating for residential buildings.

6 Results and discussion

6.1 Impact of grid Integration on the cost with different PSPS scenarios

Pareto multi-objective optimization was performed considering levelized energy cost (LEC) and grid integration (GI). The Pareto front presents all the non-dominant solutions obtained considering LEC and GI. Two scenarios were considered for the Pareto optimization: (1) with wildfire-related power shutoffs (WW) and (2) without wildfires (WOF). The WW scenario considered the period of wildfires in its year-long analysis, when the main grid is suspended during PSPS events, and the microgrid is disconnected from the main utility grid. The WOF scenario is considered a hypothetical scenario (for benchmark purposes) where the microgrid is connected to the main utility grid throughout the year. The model used for WOF is generated using a previously validated model presented in Ref. [47,53]. Therefore, WOF is used for benchmarking the WW model. The two Pareto fronts consider the scenario where the total hours of power loss for the communities due to PSPS events are 0.2% of the annual energy demand. A clear Pareto front was observed for both scenarios where costs tended to increase when reducing the grid dependency. The main difference between the two scenarios was a clear shift around $0.3/kWh, when moving from WOF to WW (Fig. 6). The cost for the WF scenario varied from $0.65–$0.75/kWh, which is notably high when considering the present electricity tariff. This clearly reflects that the cost will notably increase while using microgrids to supply power during the wildfire period with a lower PSPS (0.2% of the annual energy demand).

To assess the impact of increasing levels of PSPS (higher power supply uncertainty), Pareto optimization was performed considering LEC, grid integration level, and PSPS ratios as objective functions. The scatter and approximated contour of the Pareto front are presented in Fig. 7. A clear distribution of the Pareto solutions is observed in the objective space. However, the lines show a slight vertical gradient, suggesting that the power supply reliability (PSPS) is a more influential factor compared to the grid integration level for the LEC. For example, the region marked in dark blue having a PSPS less than 0.05% of the annual energy demand corresponds to LEC above $0.71/kWh. Similarly, the region marked in red with a PSPS above 0.3% corresponds to an LEC less than $0.52/kWh. The cost could reduce by 40% with the tolerance of power loss hours in PSPS events to be 0.3% of the annual energy demand. The results demonstrate that designing distributed energy systems operating at grid integrated mode would become expensive to alleviate the PSPS completely. On the contrary, the cost of microgrids with a certain allowance for PSPS could become quite a competitive option. Furthermore, the marginal impact of grid integration level reveals that the microgrids could be designed to operate with a much lower impact on the main utility grid.

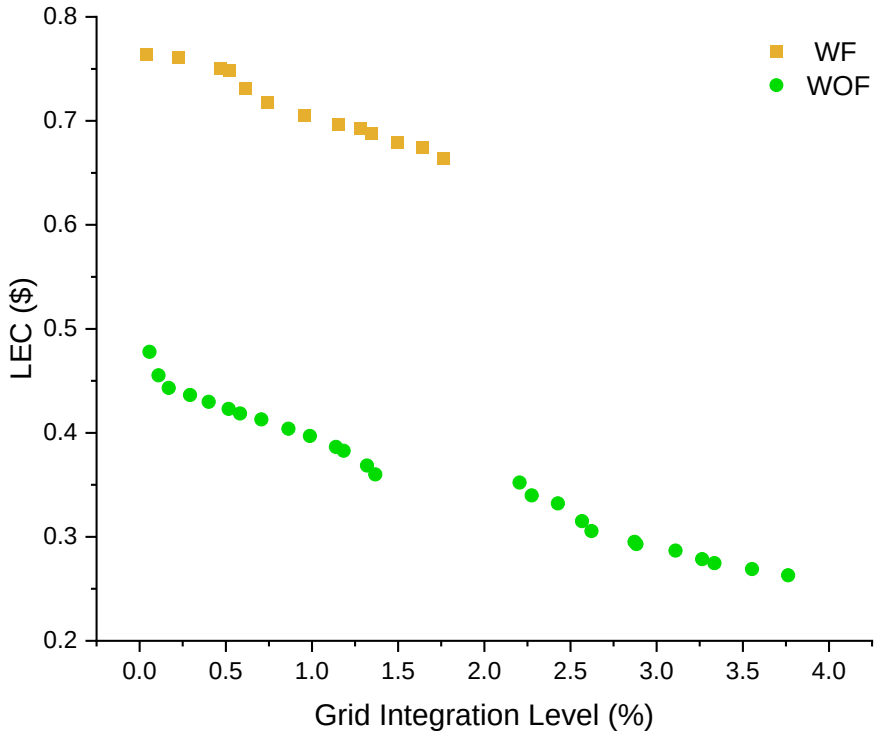

Fig. 6: Pareto fronts obtained considering levelized energy cost and grid integration as objective functions. Two scenarios were considered for the Pareto optimization: (1) with wildfires (WW) and (2) without wildfires (WOF).

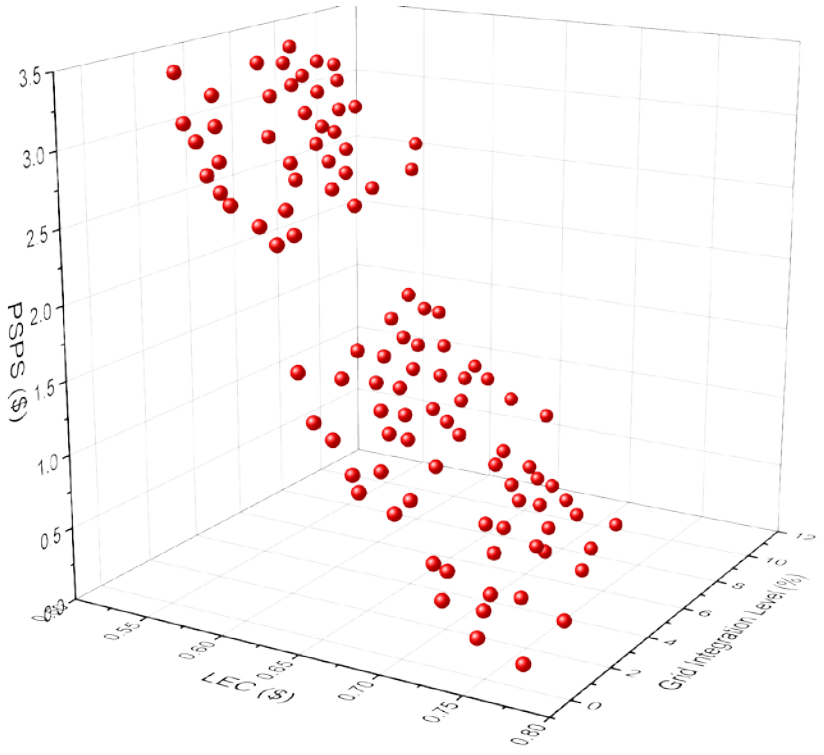

(a)

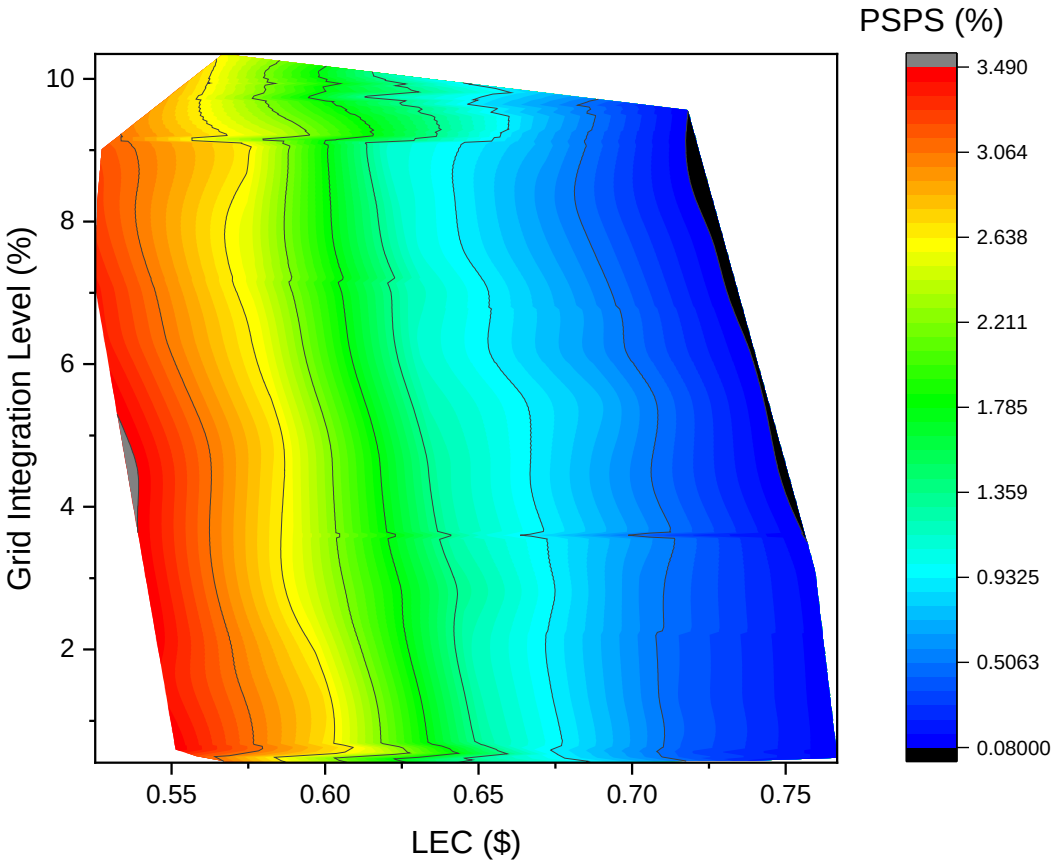

(b)

Fig. 7: (a) Scatter and (b) approximate contour plot of a 3D Pareto front considering levelized energy cost (LEC), grid integration level, and Public Safety Power Shutoffs (PSPS).

6.2 3D Pareto optimization considering cost- CO2 emissions -PSPS

A critical aspect of the distributed energy system is its capability to enhance the renewable energy penetration levels and reduce CO_2 emissions. Pareto optimization was performed considering LEC, PSPS power loss tolerance, and CO_2 emissions per kilowatt-hour to quantify the potential of the proposed microgrids to mitigate the CO_2 emissions while supplying the wildfire-prone community with reliable energy sources. The scatter and approximate contour plot of the Pareto front is presented in Fig. 8. A well-distributed Pareto front is observed, reflecting that the three objectives are conflicting. The Pareto solutions can be classified into three main classes, as shown in the approximate contour plot. Region P represents the design solutions having the lowest cost and emission levels. However, LOLP levels are higher in Region P. In contrast, Region Q represents the design solutions with higher costs and emissions. It clearly shows that the reduction in cost and CO_2 emission levels can be achieved when increasing the PSPS time. The design solutions belonging to Region Q have a higher PSPS tolerance. Region R lies between Regions P and Q and has moderate PSPS tolerance. Pareto curves are clearly observed in this region when considering cost and CO_2 emissions. The cost increases when the emission levels within Region R are attempted to be reduced. In conclusion, both cost and emission levels are adversely impacted when reducing the tolerance to PSPS-induced power loss up to a significantly lower value. However, both cost and emission levels can be notably reduced while allowing the PSPS-induced power loss time to be within 5% of the analysis period.

Seven Pareto solutions are tabulated in Table 1 to obtain a quantitative understanding of the impact of system design on the performance indicators. Design solutions within Region P (improved emissions and higher PSPS) had a lower ICG capacity, as demonstrated by Design B1. A higher renewable energy

capacity was also observed in these systems. Lower ICG and higher renewable energy capacity led to lower emission levels and a higher PSPS tolerance needed. Renewable energy generation accounted for 117% of the annual energy demand. However, a significant portion of the renewable energy generation cannot be utilized within the system. Therefore, due to storage limitations and grid curtailments, 55% of the renewable generation had to be dumped (wasted renewable energy [WRE]). As a result, utilized renewable energy generation drops up to 62 WRE levels for grid-integrated renewable energy systems were kept below 20% [47]. Therefore, Design B1 is not usually preferred as a reasonable design solution during the design phase due to the higher WRE. Design A3 in Region R showed a similar system configuration with higher renewable energy capacity and lower ICG capacity. However, A3 had a higher battery bank capacity, which reduced the PSPS from 4.98 % to 4.01 % (when moving from B1 to A3). The improvement in the reliability level came at a higher cost. The levelized cost increased from $0.60 to $0.73 (by 21%) when moving from B1 to A3. These results clearly indicate that using the battery bank to improve reliability can notably increase the cost.

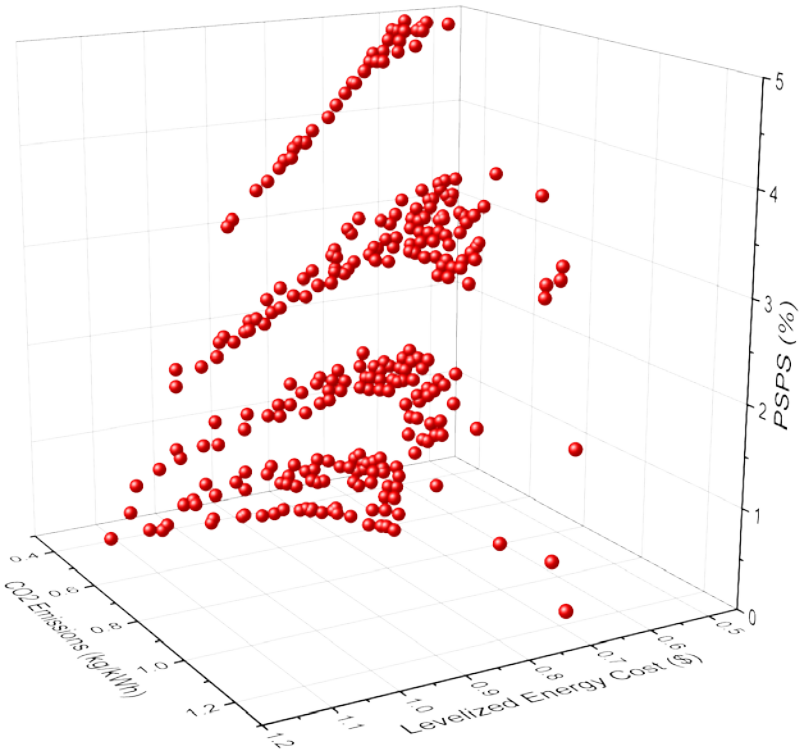

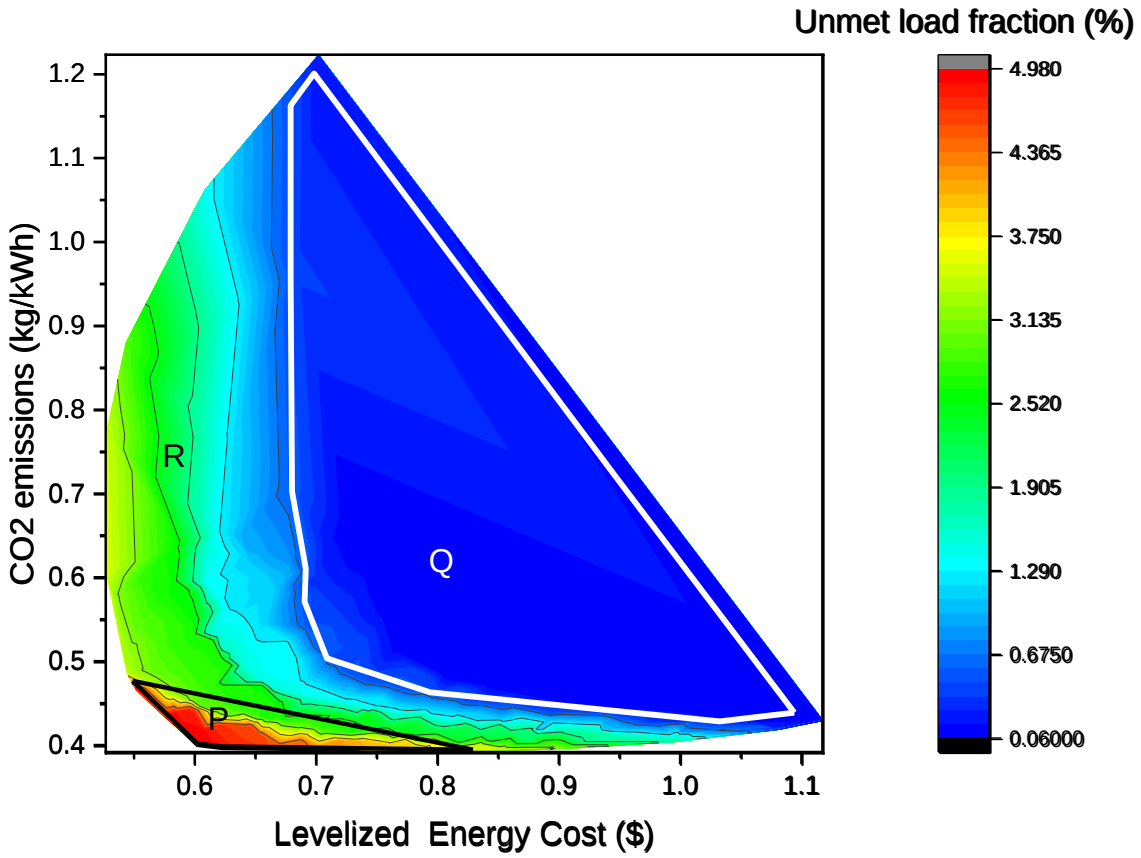

Fig. 8: (a) Scatter and (b) approximate contour plot of a 3D Pareto front considering levelized energy cost (LEC), CO_2 emission levels, and Public Safety Power Shutoffs (PSPS)

A contrasting picture can be witnessed when moving from Design B1 to C1. The PSPS reduced from 5.0% to 0.126% when moving to C1, with a notable increase in the price tag. The LEC increased from \$0.60 to \$0.84 (by 40%) when reducing the PSPS. The key difference in the system design between C1 and B1 was the increase in ICG capacity from 60 to 140 kilovolt amps (kVA). C1 has a close system configuration to design A5 in Region R. Design C1 clearly shows that reducing PSPS while maintaining a lower emission level will depend on both battery storage and the ICG, leading to increased costs. The design solutions belonging to Region R showed significant changes in both system design and performance indicators. Design A1 presents a low-cost design solution with lower ICG capacity, renewable capacity, and battery storage size. When moving from A1 to A2, the size of the battery bank increased notably, with a marginal increase in renewable energy capacity. Increased battery capacity leads to reduced CO_2 emissions. The electricity from the grid increased from 42.3% to 46.8% when moving from A1 to A2. The battery bank acts as a grid energy storage where electricity is stored in the battery bank from the grid during the normal operation of the grid and is discharged during the PSPS period. Using the battery bank as the grid storage and renewable energy integration (instead of using the ICG) reduced CO_2 emission levels by 46% (reducing emission levels by 0.771 to 0.528 kg/kWh). Design A2 reflects the impact of grid storage along with renewable energy integration when minimizing CO_2 emissions. Both renewable energy and storage capacity increased notably when moving from A2 to A3. The renewable energy capacity increased from 240 to 710 kVA. However, the grid or increased energy storage could not completely absorb fluctuations in the generation brought about by the increase in renewable energy capacity. Therefore, a significant increase in WRE took place. This clearly reflects the practical difficulties in minimizing the emission levels beyond a certain limit. Both A4 and A5 further strengthen the aforementioned points.

Table 1: Design solutions extracted from the 3D Pareto front

Design	Region	LEC ($)	CO_2 (kg/kWh)	LOLP/PSPS (%)	WRE (%)	RE Generation* (%)	From Grid (%)	RE Capacity (KVA)	Number of Battery Banks	ICG Capacity (KVA)
A1	R	0.5267	0.771	3.475	2.9	40.5	42.3	230	5	80
A2	R	0.5543	0.528	3.078	2.8	42.9	46.8	240	24	80
A3	R	0.7336	0.404	4.071	93.3	62.4	39.2	710	43	60
A4	R	0.5346	0.578	3.178	2.8	39.3	46.9	225	10	80
A5	R	0.7862	0.501	0.076	23.4	57.4	42.7	390	18	140
B1	P	0.5998	0.404	4.979	55.0	62.1	40.0	545	20	60
C1	Q	0.8416	0.471	0.126	42.9	61.3	40.6	490	19	140

6.3 Generalization of the results to multiple locations

The local conditions can notably influence the performance indicators that are discussed above. Local conditions may influence both renewable energy potential and the energy demand profile. Therefore, 3D Pareto optimization was performed considering LEC, grid integration level, and PSPS to assess the impact of local conditions and generalize the previous observations. Seven different localities named as C1-C7 were taken for comparison. Among these localities, C1 was already discussed in Sections 6.2 and 3. Among these localities, C2, C3, C4, C5, and C7 showed a notable cost reduction compared to C1 (Fig. 9(a)). C6 was the only locality that showed a notably higher LEC compared to C1. The cost distribution of C2, C3, C4, C5, and C7 are presented in Fig. 9 (b) after removing C1 and C6 clusters which can be identified as outliers when considering the cost distributions. When analyzing Fig. 9 (b), except for C4, the average cost was able to be kept below $0.3/kWh (below line T-T) while maintaining a PSPS below 2%–3%, which represents the financial feasibility of the grid-integrated microgrids. However, the cost can be notable in certain instances, such as in locality C6, where the average cost could be above $1.2. Although microgrids have become an attractive method to improve the wildfire resilience of energy infrastructure for many localities, the financial feasibility might strongly depend on local conditions that govern the renewable energy potential and the energy demand profile.

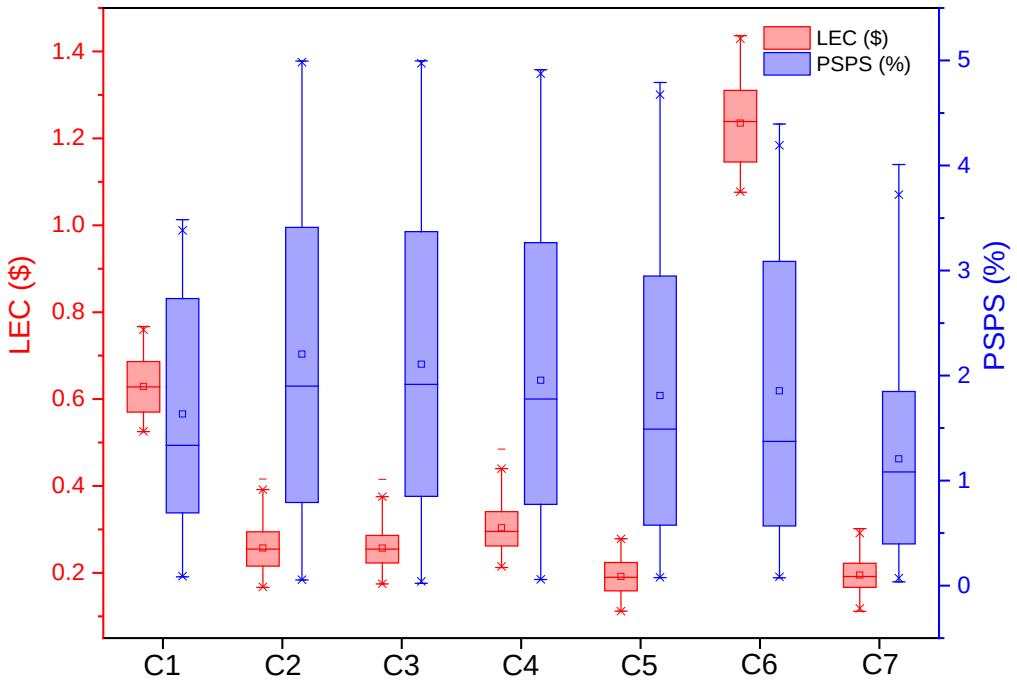

(a)

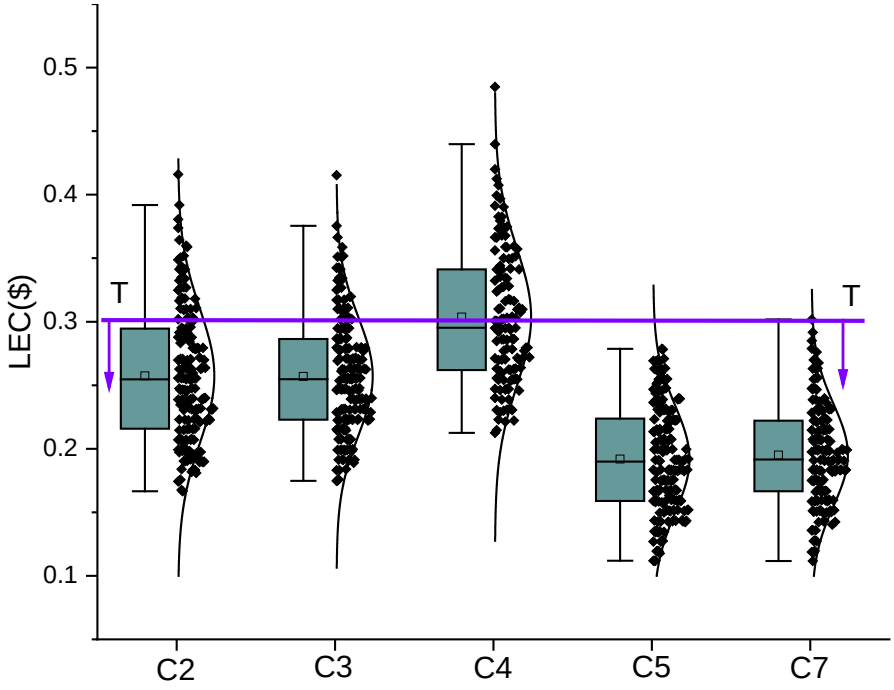

(b)

Fig. 9. The (a) double y-axis boxplot presenting PSPS and cost for the Pareto solutions. In order to facilitate further illustration, the cost distribution of localities C2, C3, C4 C5 and C7 are taken by removing the two outliers (i.e.: C1 and C6).

7 Limitations of the Study

The present study has limitations which can be addressed in future:

- Uncertainties brought up by future climate variation on energy demand and renewable energy potentials are not considered. A stochastic formulation of the objective functions may facilitate this task. The impact of uncertainties brought up by the equipment usage and occupancy on the energy demand is not considered.
- The present formulation of the net present value does not consider the cost for embodied carbon emission or salvage cost.
- Solar panel efficiency may notably degrade at the time of wildfire compared to the standard value for semi-clear or clear sky condition, which is not considered in the study.
- The present study only focuses on the design optimization of the energy system. The propagation of wildfire and the risk of damaging the components have not been considered. Locating the components of the energy system in order to minimize the risk of wildfire needs to be performed after inspecting the locality and studying the propagation of wildfires in the near vicinity.

8 Summary and conclusions

Several recent studies have proposed using microgrids to minimize the public safety power shutoffs during the wildfire period for communities at the wildland-urban interface. However, a comprehensive assessment of microgrids has not been performed to evaluate the potential to enhance resilience for communities living in the wildland-urban interface. To address this research gap, the present study introduced a novel modeling framework and assessed the potential of microgrids to enhance resilience during wildfire periods. The study revealed that

- irrespective of the differences in demand and renewable energy potential, the average levelized energy cost for microgrids could be kept below $0.3/kWh while maintaining public safety power shutoffs below 2%–3% for most communities.
- The renewable energy penetration level (both solar and wind) could increase up to 60% of the annual energy demand, decreasing CO_2 emissions to 0.4 kg/kWh.
- Energy storage plays a vital role in reducing CO_2 emissions, as well as in minimizing the public safety power shutoffs.
- Although microgrids could limit the public safety power shutoffs up to 2%–3% of the annual energy demand, eliminating it completely would become challenging. This is because it would notably increase the cost as well as renewable energy generation that cannot be utilized (wasted renewable energy generation due to curtailments). The higher cost of energy storage becomes the bottleneck when eliminating the public safety power shutoffs, which will be addressed in the near future with the advancement in energy storage technologies.

Finally, we recommend microgrids as an attractive method to minimize public safety power shutoffs and enhance the climate resilience of energy infrastructure for communities living in the wildland-urban interface. We hope that improvement in renewable energy penetration levels and a reduction in CO_2 emissions brought by microgrids will convince authorities to adopt this technology.

Acknowledgment: This work was supported in part by the Project of Hetao Shenzhen-Hong Kong Science and Technology Innovation Cooperation Zone (HZQB-KCZYB-2020083)

References

[1] Environment UN. Spreading like Wildfire: The Rising Threat of Extraordinary Landscape Fires. UNEP - UN Environment Programme 2022. http://www.unep.org/resources/report/spreading-wildfire-rising-threat-extraordinary-landscape-fires (accessed August 17, 2022).

[2] Perera ATD, Hong T. Vulnerability and resilience of urban energy ecosystems to extreme climate events: A systematic review and perspectives. Renewable and Sustainable Energy Reviews 2023;173:113038. https://doi.org/10.1016/j.rser.2022.113038.

[3] Nik VM, Perera ATD, Chen D. Towards climate resilient urban energy systems: a review. National Science Review 2021;8. https://doi.org/10.1093/nsr/nwaa134.

[4] Perera ATD, Nik VM, Chen D, Scartezzini J-L, Hong T. Quantifying the impacts of climate change and extreme climate events on energy systems. Nature Energy 2020;5:150–9. https://doi.org/10.1038/s41560-020-0558-0.

[5] Sun K, Zhang W, Zeng Z, Levinson R, Wei M, Hong T. Passive cooling designs to improve heat resilience of homes in underserved and vulnerable communities. Energy and Buildings 2021;252:111383. https://doi.org/10.1016/j.enbuild.2021.111383.

[6] Zeng Z, Zhang W, Sun K, Wei M, Hong T. Investigation of pre-cooling as a recommended measure to improve residential buildings' thermal resilience during heat waves. Building and Environment 2022;210:108694. https://doi.org/10.1016/j.buildenv.2021.108694.

[7] Florida nursing home hit by Hurricane Irma: 4 charged in 12 deaths n.d. https://www.usatoday.com/story/news/nation/2019/08/27/florida-nursing-home-hurricane-irma-4-charged-12-deaths/2136076001/ (accessed December 23, 2022).

[8] Sun K, Specian M, Hong T. Nexus of thermal resilience and energy efficiency in buildings: A case study of a nursing home. Building and Environment 2020;177:106842. https://doi.org/10.1016/j.buildenv.2020.106842.

[9] Wang Z, Hong T, Li H. Informing the planning of rotating power outages in heat waves through data analytics of connected smart thermostats for residential buildings. Environ Res Lett 2021;16:074003. https://doi.org/10.1088/1748-9326/ac092f.

[10] What is the WUI? US Fire Administration 2022. https://www.usfa.fema.gov/wui/what-is-the-wui.html (accessed August 17, 2022).

[11] List of California wildfires. Wikipedia 2022.

[12] Romanello M, McGushin A, Napoli CD, Drummond P, Hughes N, Jamart L, et al. The 2021 report of the Lancet Countdown on health and climate change: code red for a healthy future. The Lancet 2021;398:1619–62. https://doi.org/10.1016/S0140-6736(21)01787-6.

[13] How Microgrids Work. EnergyGov n.d. https://www.energy.gov/articles/how-microgrids-work (accessed August 17, 2022).

[14] Luber G, McGeehin M. Climate Change and Extreme Heat Events. American Journal of Preventive Medicine 2008;35:429–35. https://doi.org/10.1016/j.amepre.2008.08.021.

[15] Knowlton K, Rotkin -Ellman Miriam, King G, Margolis HG, Smith D, Solomon G, et al. The 2006 California Heat Wave: Impacts on Hospitalizations and Emergency Department Visits. Environmental Health Perspectives 2009;117:61–7. https://doi.org/10.1289/ehp.11594.

[16] Merte S. Estimating heat wave-related mortality in Europe using singular spectrum analysis. Climatic Change 2017;142:321–30. https://doi.org/10.1007/s10584-017-1937-9.

[17] Mottahedi A, Sereshki F, Ataei M, Nouri Qarahasanlou A, Barabadi A. The Resilience of Critical Infrastructure Systems: A Systematic Literature Review. Energies 2021;14:1571. https://doi.org/10.3390/en14061571.

[18] Jazebi S, de León F, Nelson A. Review of Wildfire Management Techniques—Part I: Causes, Prevention, Detection, Suppression, and Data Analytics. IEEE Transactions on Power Delivery 2020;35:430–9. https://doi.org/10.1109/TPWRD.2019.2930055.

[19] Nazaripouya H. Power Grid Resilience under Wildfire: A Review on Challenges and Solutions. 2020 IEEE Power Energy Society General Meeting (PESGM), 2020, p. 1–5. https://doi.org/10.1109/PESGM41954.2020.9281708.

[20] Sathaye JA, Dale LL, Larsen PH, Fitts GA, Koy K, Lewis SM, et al. Rising Temps, Tides, and Wildfires: Assessing the Risk to California's Energy Infrastructure from Projected Climate Change. IEEE Power and Energy Magazine 2013;11:32–45. https://doi.org/10.1109/MPE.2013.2245582.
[21] Rhodes N, Ntaimo L, Roald L. Balancing Wildfire Risk and Power Outages Through Optimized Power Shut-Offs. IEEE Transactions on Power Systems 2021;36:3118–28. https://doi.org/10.1109/TPWRS.2020.3046796.
[22] Koufakis EI, Tsarabaris PT, Katsanis JS, Karagiannopoulos CG, Bourkas PD. A Wildfire Model for the Estimation of the Temperature Rise of an Overhead Line Conductor. IEEE Transactions on Power Delivery 2010;25:1077–82. https://doi.org/10.1109/TPWRD.2009.2035128.
[23] Muhs J, Parvania M, Nguyen HT, Palmer JA. Characterizing Probability of Wildfire Ignition Caused by Power Distribution Lines. IEEE Transactions on Power Delivery 2020:1–1. https://doi.org/10.1109/TPWRD.2020.3047101.
[24] Wischkaemper JA, Benner CL, Don Russell B, Muthu Manivannan K. Application of advanced electrical waveform monitoring and analytics for reduction of wildfire risk. ISGT 2014, 2014, p. 1–5. https://doi.org/10.1109/ISGT.2014.6816487.
[25] Mohagheghi S, Rebennack S. Optimal resilient power grid operation during the course of a progressing wildfire. International Journal of Electrical Power & Energy Systems 2015;73:843–52. https://doi.org/10.1016/j.ijepes.2015.05.035.
[26] Trakas DN, Hatziargyriou ND. Optimal Distribution System Operation for Enhancing Resilience Against Wildfires. IEEE Transactions on Power Systems 2018;33:2260–71. https://doi.org/10.1109/TPWRS.2017.2733224.
[27] Tandon S, Grijalva S, Molzahn DK. Motivating the Use of Dynamic Line Ratings to Mitigate the Risk of Wildfire Ignition. 2021 IEEE Power and Energy Conference at Illinois (PECI), 2021, p. 1–7. https://doi.org/10.1109/PECI51586.2021.9435252.
[28] Hay C, Chhabra M. The impact of wildfires and beneficial electrification on electricity rates in PG&E's service territory. The Electricity Journal 2020;33:106710. https://doi.org/10.1016/j.tej.2020.106710.
[29] 2021 WILDFIRE MITIGATION PLAN REPORT 2021:1013.
[30] Schoolov K. How PG&E is fighting its massive wildfire problem with microgrids, power shutoffs and cutting down trees. CNBC 2021. https://www.cnbc.com/2021/07/03/how-californias-pge-is-fighting-its-massive-wildfire-problem.html (accessed February 15, 2022).
[31] Alruwaili M, Cipcigan L. Optimal Annual Operational Cost of a Hybrid Renewable-Based Microgrid to Increase the Power Resilience of a Critical Facility. Energies 2022;15:8040. https://doi.org/10.3390/en15218040.
[32] Yang W, Sparrow SN, Ashtine M, Wallom DCH, Morstyn T. Resilient by design: Preventing wildfires and blackouts with microgrids. Applied Energy 2022;313:118793. https://doi.org/10.1016/j.apenergy.2022.118793.
[33] Moreno R, Trakas DN, Jamieson M, Panteli M, Mancarella P, Strbac G, et al. Microgrids Against Wildfires: Distributed Energy Resources Enhance System Resilience. IEEE Power and Energy Magazine 2022;20:78–89. https://doi.org/10.1109/MPE.2021.3122772.
[34] Hanna R. Optimal Investment in Microgrids to Mitigate Power Outages from Public Safety Power Shutoffs. 2021 IEEE Power & Energy Society General Meeting (PESGM), 2021, p. 1–5. https://doi.org/10.1109/PESGM46819.2021.9637923.
[35] Perera ATD, Wickremasinghe DMIJ, Mahindarathna DVS, Attalage RA, Perera KKCK, Bartholameuz EM. Sensitivity of internal combustion generator capacity in standalone hybrid energy systems. Energy 2012;39:403–11. https://doi.org/10.1016/j.energy.2011.12.039.
[36] Perera ATD, Madusanka AN, Attalage RA, Perera KKCK. A multi criterion analysis for renewable energy integration process of a standalone hybrid energy system with internal combustion generator. Journal of Renewable and Sustainable Energy 2015;7:043128. https://doi.org/10.1063/1.4928684.

[37] Development of Residential Prototype Building Models and Analysis System for Large-Scale Energy Efficiency Studies Using EnergyPlus | PNNL n.d. https://www.pnnl.gov/publications/development-residential-prototype-building-models-and-analysis-system-large-scale (accessed August 17, 2022).
[38] Notton G, Lazarov V, Stoyanov L. Optimal sizing of a grid-connected PV system for various PV module technologies and inclinations, inverter efficiency characteristics and locations. Renewable Energy 2010;35:541–54. https://doi.org/10.1016/j.renene.2009.07.013.
[39] Hocaoğlu FO, Gerek ÖN, Kurban M. A novel hybrid (wind–photovoltaic) system sizing procedure. Solar Energy 2009;83:2019–28. https://doi.org/10.1016/j.solener.2009.07.010.
[40] Diaf S, Diaf D, Belhamel M, Haddadi M, Louche A. A methodology for optimal sizing of autonomous hybrid PV/wind system. Energy Policy 2007;35:5708–18. https://doi.org/10.1016/j.enpol.2007.06.020.
[41] Perera ATD, Nik VM, Wickramasinghe PU, Scartezzini J-L. Redefining energy system flexibility for distributed energy system design. Applied Energy 2019;253. https://doi.org/10.1016/j.apenergy.2019.113572.
[42] Perera ATD, Attalage RA, Perera KKCK, Dassanayake VPC. Designing standalone hybrid energy systems minimizing initial investment, life cycle cost and pollutant emission. Energy 2013;54:220–30. https://doi.org/10.1016/j.energy.2013.03.028.
[43] Downing SD, Socie DF. Simple rainflow counting algorithms. International Journal of Fatigue 1982;4:31–40. https://doi.org/10.1016/0142-1123(82)90018-4.
[44] Perera ATD, Wickramasinghe PU, Nik VM, Scartezzini J-L. Introducing reinforcement learning to the energy system design process. Applied Energy 2020;262:114580. https://doi.org/10.1016/j.apenergy.2020.114580.
[45] Perera ATD, Kamalaruban P. Applications of reinforcement learning in energy systems. Renewable and Sustainable Energy Reviews 2021;137:110618. https://doi.org/10.1016/j.rser.2020.110618.
[46] Mohammed A, Pasupuleti J, Khatib T, Elmenreich W. A review of process and operational system control of hybrid photovoltaic/diesel generator systems. Renewable and Sustainable Energy Reviews 2015;44:436–46. https://doi.org/10.1016/j.rser.2014.12.035.
[47] Perera ATD, Nik VM, Mauree D, Scartezzini J-L. Electrical hubs: An effective way to integrate non-dispatchable renewable energy sources with minimum impact to the grid. Applied Energy 2017;190:232–48. https://doi.org/10.1016/j.apenergy.2016.12.127.
[48] Dufolopez R, Bernalagustin J. Design and control strategies of PV-Diesel systems using genetic algorithms. Solar Energy 2005;79:33–46. https://doi.org/10.1016/j.solener.2004.10.004.
[49] Perera ATD, Attalage RA, Perera KKCK, Dassanayake VPC. A hybrid tool to combine multi-objective optimization and multi-criterion decision making in designing standalone hybrid energy systems. Applied Energy 2013;107:412–25. https://doi.org/10.1016/j.apenergy.2013.02.049.
[50] Takagi T, Sugeno M. Fuzzy identification of systems and its applications to modeling and control. IEEE Transactions on Systems, Man, and Cybernetics 1985;SMC-15:116–32. https://doi.org/10.1109/TSMC.1985.6313399.
[51] Sugeno M. An introductory survey of fuzzy control. Information Sciences 1985;36:59–83. https://doi.org/10.1016/0020-0255(85)90026-X.
[52] Sugeno M, Kang GT. Structure identification of fuzzy model. Fuzzy Sets and Systems 1988;28:15–33. https://doi.org/10.1016/0165-0114(88)90113-3.
[53] Perera ATD, Nik VM, Mauree D, Scartezzini J-L. An integrated approach to design site specific distributed electrical hubs combining optimization, multi-criterion assessment and decision making. Energy 2017;134:103–20. https://doi.org/10.1016/j.energy.2017.06.002.
[54] Barley CD, Winn CB. Optimal dispatch strategy in remote hybrid power systems. Solar Energy 1996;58:165–79.

[55] Celik AN. Effect of different load profiles on the loss-of-load probability of stand-alone photovoltaic systems. Renewable Energy 2007;32:2096–115. https://doi.org/10.1016/j.renene.2006.11.002.
[56] Abbes D, Martinez A, Champenois G. Life cycle cost, embodied energy and loss of power supply probability for the optimal design of hybrid power systems. Mathematics and Computers in Simulation 2014;98:46–62. https://doi.org/10.1016/j.matcom.2013.05.004.
[57] Hadj Arab A, Chenlo F, Benghanem M. Loss-of-load probability of photovoltaic water pumping systems. Solar Energy 2004;76:713–23. https://doi.org/10.1016/j.solener.2004.01.006.
[58] Heydari A, Askarzadeh A. Optimization of a biomass-based photovoltaic power plant for an off-grid application subject to loss of power supply probability concept. Applied Energy 2016;165:601–11. https://doi.org/10.1016/j.apenergy.2015.12.095.
[59] Laumanns M, Thiele L, Deb K, Zitzler E. Combining Convergence and Diversity in Evolutionary Multiobjective Optimization. Evolutionary Computation 2002;10:263–82. https://doi.org/10.1162/106365602760234108.
[60] Deb K. An efficient constraint handling method for genetic algorithms. Computer Methods in Applied Mechanics and Engineering 2000;186:311–38. https://doi.org/10.1016/S0045-7825(99)00389-8.
[61] Deb K, Beyer H-G. Self-Adaptive Genetic Algorithms with Simulated Binary Crossover. Evolutionary Computation 2001;9:197–221. https://doi.org/10.1162/106365601750190406.
[62] Qin AK, Huang VL, Suganthan PN. Differential Evolution Algorithm With Strategy Adaptation for Global Numerical Optimization. IEEE Transactions on Evolutionary Computation 2009;13:398–417. https://doi.org/10.1109/TEVC.2008.927706.
[63] Storn R, Price K. Differential Evolution – A Simple and Efficient Heuristic for global Optimization over Continuous Spaces. Journal of Global Optimization n.d.;11:341–59. https://doi.org/10.1023/A:1008202821328.
[64] Brest J, Greiner S, Boskovic B, Mernik M, Zumer V. Self-Adapting Control Parameters in Differential Evolution: A Comparative Study on Numerical Benchmark Problems. IEEE Transactions on Evolutionary Computation 2006;10:646–57. https://doi.org/10.1109/TEVC.2006.872133.
[65] Perera ATD, Nik VM, Mauree D, Scartezzini J-L. Electrical hubs: An effective way to integrate non-dispatchable renewable energy sources with minimum impact to the grid. Applied Energy 2017;190:232–48. https://doi.org/10.1016/j.apenergy.2016.12.127.
[66] Perera ATD, Attalage RA, Perera KKCK, Dassanayake VPC. A hybrid tool to combine multi-objective optimization and multi-criterion decision making in designing standalone hybrid energy systems. Applied Energy 2013;107:412–25. https://doi.org/10.1016/j.apenergy.2013.02.049.
[67] Perera ATD, Wang Z, Nik VM, Scartezzini J-L. Towards realization of an Energy Internet: Designing distributed energy systems using game-theoretic approach. Applied Energy 2021;283:116349. https://doi.org/10.1016/j.apenergy.2020.116349.
[68] Perera ATD, Javanroodi K, Wang Y, Hong T. Urban cells: Extending the energy hub concept to facilitate sector and spatial coupling. Advances in Applied Energy 2021;3:100046. https://doi.org/10.1016/j.adapen.2021.100046.
[69] Wang Z, Perera ATD. Integrated platform to design robust energy internet. Applied Energy 2020;269:114942. https://doi.org/10.1016/j.apenergy.2020.114942.
[70] microsoft/USBuildingFootprints 2022.
[71] Fire Hazard Severity Zones Maps n.d. https://osfm.fire.ca.gov/divisions/community-wildfire-preparedness-and-mitigation/wildland-hazards-building-codes/fire-hazard-severity-zones-maps/ (accessed August 17, 2022).
[72] WINDExchange: California Offshore 90-Meter Wind Map and Wind Resource Potential n.d. https://windexchange.energy.gov/maps-data/146 (accessed August 17, 2022).